NASA/CR-2002-211650

Revolutionary Concepts for Helicopter Noise Reduction — S.I.L.E.N.T. Program

Bryan Edwards and Charles Cox
Bell Helicopter Textron Inc., Fort Worth, Texas

May 2002

The NASA STI Program Office . . . in Profile

Since its founding, NASA has been dedicated to the advancement of aeronautics and space science. The NASA Scientific and Technical Information (STI) Program Office plays a key part in helping NASA maintain this important role.

The NASA STI Program Office is operated by Langley Research Center, the lead center for NASA's scientific and technical information. The NASA STI Program Office provides access to the NASA STI Database, the largest collection of aeronautical and space science STI in the world. The Program Office is also NASA's institutional mechanism for disseminating the results of its research and development activities. These results are published by NASA in the NASA STI Report Series, which includes the following report types:

- TECHNICAL PUBLICATION. Reports of completed research or a major significant phase of research that present the results of NASA programs and include extensive data or theoretical analysis. Includes compilations of significant scientific and technical data and information deemed to be of continuing reference value. NASA counterpart of peer-reviewed formal professional papers, but having less stringent limitations on manuscript length and extent of graphic presentations.

- TECHNICAL MEMORANDUM. Scientific and technical findings that are preliminary or of specialized interest, e.g., quick release reports, working papers, and bibliographies that contain minimal annotation. Does not contain extensive analysis.

- CONTRACTOR REPORT. Scientific and technical findings by NASA-sponsored contractors and grantees.

- CONFERENCE PUBLICATION. Collected papers from scientific and technical conferences, symposia, seminars, or other meetings sponsored or co-sponsored by NASA.

- SPECIAL PUBLICATION. Scientific, technical, or historical information from NASA programs, projects, and missions, often concerned with subjects having substantial public interest.

TECHNICAL TRANSLATION. English-language translations of foreign scientific and technical material pertinent to NASA's mission.

Specialized services that complement the STI Program Office's diverse offerings include creating custom thesauri, building customized databases, organizing and publishing research results . . . even providing videos.

For more information about the NASA STI Program Office, see the following:

- Access the NASA STI Program Home Page at ***http://www.sti.nasa.gov***

- Email your question via the Internet to help@sti.nasa.gov

- Fax your question to the NASA STI Help Desk at (301) 621-0134

- Telephone the NASA STI Help Desk at (301) 621-0390

- Write to:
  NASA STI Help Desk
  NASA Center for AeroSpace Information
  7121 Standard Drive
  Hanover, MD 21076-1320

ERRATA

NASA/CR-2002-211650

Revolutionary Concepts for Helicopter Noise Reduction — S.I.L.E.N.T. Program

Bryan Edwards and Charles Cox

May 2002

An error occurred on the Title Page of this report.

A corrected copy of the report is attached. Please destroy all copies previously sent to you.

Issued June 2002

NASA/CR-2002-211650

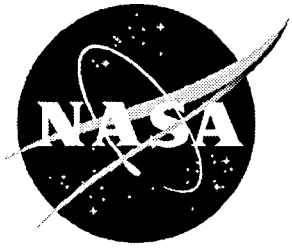

Revolutionary Concepts for Helicopter Noise Reduction — S.I.L.E.N.T. Program

Bryan Edwards and Charles Cox
Bell Helicopter Textron Inc., Fort Worth, Texas

National Aeronautics and
Space Administration

Langley Research Center
Hampton, Virginia 23681-2199

Prepared for Langley Research Center
under Contract NAS1-99109

May 2002

Available from:

NASA Center for AeroSpace Information (CASI)
7121 Standard Drive
Hanover, MD 21076-1320
(301) 621-0390

National Technical Information Service (NTIS)
5285 Port Royal Road
Springfield, VA 22161-2171
(703) 605-6000

TABLE OF CONTENTS

LIST OF FIGURES

LIST OF TABLES

1. ABSTRACT

As part of a NASA initiative to reduce helicopter main rotor noise, a Phase 1 study has been performed of candidate noise reduction concepts. Both conventional and novel design technologies have been analyzed that reduce the community impact of helicopter operations. In this study the noise reduction potential and design implications are assessed for conventional means of noise reduction, e.g., tip speed reduction, tip shapes and airfoil tailoring, and for two innovative design concepts: *modulated blade spacing* and *x-force control.* Main rotor designs that incorporate *modulated blade spacing* are shown to have reduced peak noise levels in most flight operations. *X-force control* alters the helicopter's force balance whereby the miss distance between main rotor blades and shed vortices can be controlled. This control provides a high potential to mitigate BVI noise radiation. Each concept is evaluated using best practice design and analysis methods, achieving the study's aim to significantly reduce noise with minimal performance degradation and no vibration increase. It is concluded that a SILENT main rotor design, incorporating the *modulated blade spacing* concept, offers significantly reduced noise levels and the potential of a break-through in how a helicopter's sound is perceived and judged. The SILENT rotor represents a definite advancement in the state-of-the-art and is selected as the design concept for demonstration in Phase 2. A Phase 2 Implementation Plan is developed for whirl cage and wind tunnel evaluations of a scaled model SILENT rotor.

2. INTRODUCTION AND BACKGROUND

The continued growth of commercial reliance upon the rotorcraft industry has brought about the need for noise reduction technology. The occurrence of rotorcraft operations in and near population centers is increasing, with a corresponding heightened public awareness of, and in a growing number of instances, an adverse response to the noise associated with these operations. In greater and greater numbers, rotorcraft operations are being constrained by local governments responding to public pressure. Local ordinances impose or attempt to impose restrictions on the frequency of operations, flight path utilization, time of day of specific operations, and types of rotorcraft used. Additionally, regulatory bodies are imposing more stringent noise specifications as a requirement for civil certification of rotorcraft.

Demand for lower noise levels is becoming stronger in all markets. The growing European market is particularly sensitive, but portions of the domestic market are also requiring substantial noise reduction. In recent years, helicopter tour operators in the U.S. have been increasingly restricted by the National Park Service to preserve the "natural quiet" in all national parks.

Continued growth of the rotorcraft industry also requires expansion of the supporting infrastructure. Whenever construction of a new landing/take-off terminal area (helistop, helipad, heliport, or vertiport) is being considered near a population center, public hearings are conducted prior to approval by the local regulatory bodies. Noise impact is invariably a subject of emotionally charged discussions at such hearings. In a great percentage of such cases, it is also the cause for denial of a permit by the regulatory body. Such examples serve as a gauge of the public attitude toward rotorcraft noise, and also illustrates an area in which growth of the rotorcraft industry is being increasingly restricted for reasons of noise.

Rotorcraft operators have generally responded to this growing public awareness by modifying operations of their existing fleet to minimize community noise impact. In some instances, these modifications involve the use of known "Fly Neighborly" techniques and modifications to flight paths in an attempt to minimize the noise "footprint." In other cases, the number of operations and the operating times are restricted. These sometimes work counter to the profitability of the operation, and in extreme cases can force an operator out of a particular service market. Having done all he can with the rotorcraft currently in his fleet, the operator turns to the rotorcraft manufacturer with a renewed demand for quieter aircraft.

The manufacturer responds to the operator's demands by incorporating proven noise-reduction technology into his product. The manufacturer is also constrained by market forces and the internal demand for profitability. Current technology for noise reduction, if it is to be employed in new rotorcraft designs, must ensure that the cost, performance, and other market impositions on the design are met in concert with reduced noise.

2.1 Objectives and Goals

The NASA Aeronautics and Space Technology Enterprise goals, in Pillar 1 - Global Civil Aviation, are to reduce perceived noise levels of future aircraft by a factor of 2 from today's subsonic aircraft within 10 years and by a factor of 4 within 20 years. The current study supports these goals specifically for future helicopters and, by similarity, for future tiltrotor aircraft. The study's noise reduction targets are:

- at least 8 dBA relative to an appropriate baseline design for maximum noise level occurring anywhere on the ground when the vehicle is at an altitude of 120m during an approach condition representative of noise certification (i.e., 6-deg. descent at constant airspeed),

- at least 3 dBA during climb, and

- at least 3 dBA relative to the same baseline for the maximum noise level occurring anywhere on the ground when the vehicle is at an altitude of 150m in level flyover.

The objective of this Phase 1 study is to develop innovative design concepts for helicopter noise reduction to lessen the community impact of helicopter operations in and over populated areas, such as communities near heliports. The goals are to assess low-noise technology design concepts and to determine noise reduction potential by computation, analysis, and prediction in Phase 1, followed by a demonstration test program in Phase 2.

As new and innovative means of reducing helicopter noise are identified, and their design implications documented, the likelihood increases that these low-noise concepts will be applied to future helicopter designs. It is anticipated that many of these solutions will also be applicable to tiltrotor aircraft. A long-range goal of demonstrating a quiet rotor on one or more tiltrotor aircraft testbeds is expected to benefit from the results of this study.

2.2 Noise Generation

For the conventional helicopter, there are two fundamental systems that contribute to the generation of near-field and far-field noise, the main rotor and the tail rotor. Each rotor emits unique and recognizable sounds due to its highly individualized operating condition. Engine noise is typically of secondary significance. Figure 2-1 illustrates the numerous noise sources and generating mechanisms present in a helicopter and their spectral contents. For purposes of this study, the focus is on the primary main rotor noise sources and generating mechanisms.

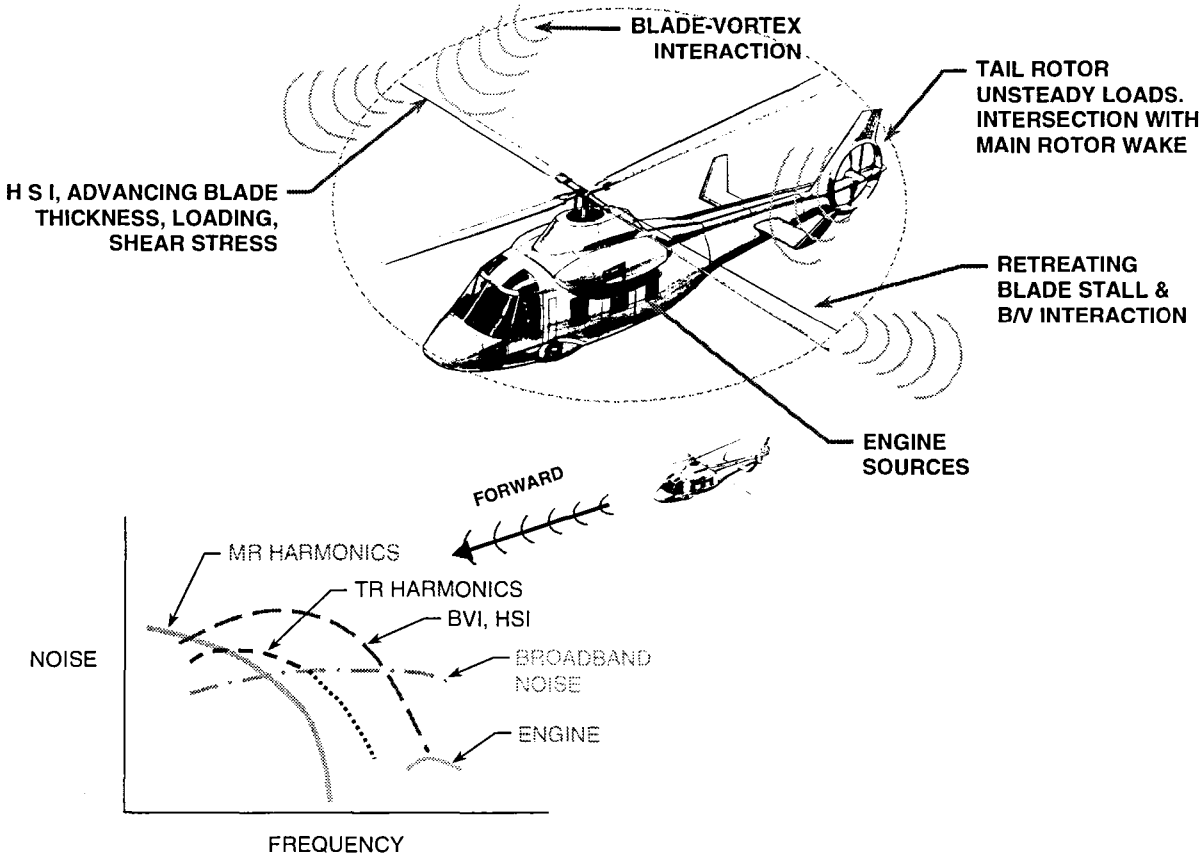

Figure 2-1. Helicopter noise propagates from numerous sources

A helicopter main rotor generates primarily low frequency noise and, in certain operating regimes, high amplitude low-to-mid-frequency noise modulated at the blade passage frequency. The low frequency rotor noise is made up of basic loading noise and broadband turbulence noise, each a function of lift and rotational speed. These sources are present in any lifting rotor. Additional sources, such as Blade Vortex Interaction (BVI) noise and High Speed Impulsive (HSI) noise, become dominant in specific operating regimes, namely in descents and at high forward airspeeds, respectively.

BVI noise can be the most significant contributor, because it occurs during a helicopter's approach to the terminal area. If the terminal is located in areas of high population density, the community will experience increased noise exposure. BVI noise is the impulsive sound emitted when a rotating blade's aerodynamic forces rapidly fluctuate during an interaction with vortices shed from the blade tip.

The severity of main rotor noise can also increase during en-route operations due to compressibility effects under high-speed flow conditions. This HSI noise is created by a "de-

localization" of high-speed transonic flow, resulting in impulsive wave-fronts from each blade that propagate into the acoustic far-field.

Each main rotor noise source mechanism has a distinct directivity pattern, as illustrated in Figure 2-2. Basic loading noise during hover is generally dominant in a conical region directed 30 to 40 degrees downward from the rotor plane, while broad-band noise radiates mostly out of the plane of the rotor. HSI noise, which is an extreme case of thickness noise, occurs on the advancing side and propagates strongly forward, but manifests itself primarily in the rotor disk plane. BVI noise also occurs on the advancing side of the rotor disk and has a strong component below and ahead of the rotor.

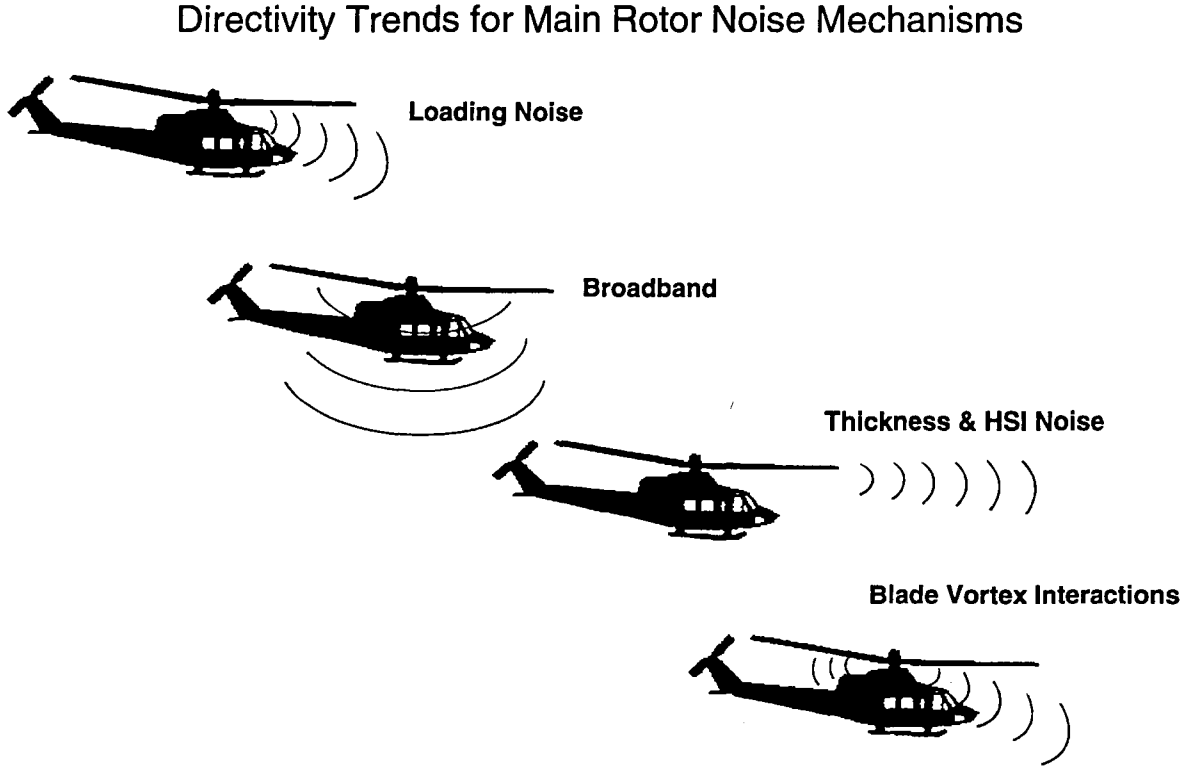

Figure 2-2. Each noise source has a unique directivity trend

3. PHASE 1 NOISE REDUCTION DESIGN STUDY

Control of main rotor noise has traditionally been accomplished by the judicious selection of rotor blade configurations and rotational tip speed. Airfoils, blade planforms, and tip shapes are chosen which mitigate the effects of HSI noise and BVI noise. For a given design gross weight, increasing the blade chord and changing the number of rotor blades are means of reaching an acoustically desirable rotational tip speed. The blade number change also alters the frequency distribution of the sound generated.

The most direct method of controlling BVI noise is by reducing or diffusing the tip vortex. Tip shapes such as the sub-wing, Ogee tip, and others have been shown to cause measurable reductions in BVI noise by modifying the vortex structure. BVI noise can also be mitigated by on-board controls that alter the physical distance between blade and shed vortices or vary the effective blade angle-of-attack. Higher harmonic control (HHC) and individual blade control (IBC) are examples of such controls.

One innovative means of reducing rotor noise is that of *modulated blade spacing*, i.e., spacing the blades unevenly. Equal blade spacing causes the fundamental frequency and its harmonics to each reinforce one another, and thus adversely affect the perceived noise. Uneven or *modulated blade spacing* skews the acoustic energy into several fundamental frequencies, with the harmonics of each being similarly skewed. In the latter case, the perceived noise can be significantly less, as has been demonstrated in anti-torque systems such as ducted fans and tail rotors.

Another innovative means of reducing rotor noise, specifically BVI noise, is by the use of *X-force control* in the non-rotating system to modify the vortex path with respect to the rotor plane, and thus to modify the inflow angle during descent. This concept requires a means of controlling drag during descent, such as a mechanism attached to the non-rotating (fuselage) structure. This promises a distinct advantage over the relative complexity of on-blade controls.

3.1 Preliminary Assessment of Concepts

A preliminary assessment of each main rotor noise reduction concept has been made and is discussed in this section. First level analyses of some of the concepts include the prediction of the noise reduction potential and identification of significant noise reduction in which there is minimal performance impact and no vibration increase. The assessment also identifies the potential for advancement in the state of the art and considerations for implementing hardware. Noise reduction candidates are summarized, leading to rationale for a down-select activity.

3.1.1 Modulated Blade Spacing

Helicopter main rotors have historically been designed with equally spaced blades. This equal spacing from one blade to the next translates to a main rotor acoustic spectrum characterized by a single fundamental blade-passage frequency and its harmonics. As many as 20 or 30 harmonics are commonly present in a main rotor's acoustic spectrum, each of which is a multiple of the fundamental blade-passage frequency. In a typical spectral plot, these frequencies appear as pronounced, ordered "peaks" spread evenly across the acoustic spectrum.

Since the acoustic frequencies associated with the rotating blades are directly related to the blade spacing, intuitively the use of unevenly spaced blades holds the potential of lower sound levels and less perceptibility. The acoustic effect of uneven or *modulated blade spacing* is to generate several blade-passage frequencies, one for each unique angle between blades. Each blade passage frequency, in turn, generates its own set of harmonics. The total acoustic energy is thereby spread over a broader range of frequencies, rather than being concentrated at one blade-passage frequency and a single set of harmonics.

The *modulated blade spacing* concept has been convincingly demonstrated in whirl stand and flight tests of ducted tail rotor configurations (References 1-3). Figure 3-1 illustrates the concept and its influence on the acoustic spectrum. The acoustic benefits are two-fold: lower peak sounds which translate into reduced dBA and SEL levels, and four or more times the number of source frequencies which in turn share the acoustic energy. In addition, a dramatic improvement in sound quality results, as witnessed during the testing and in comparative playbacks of the sound recordings.

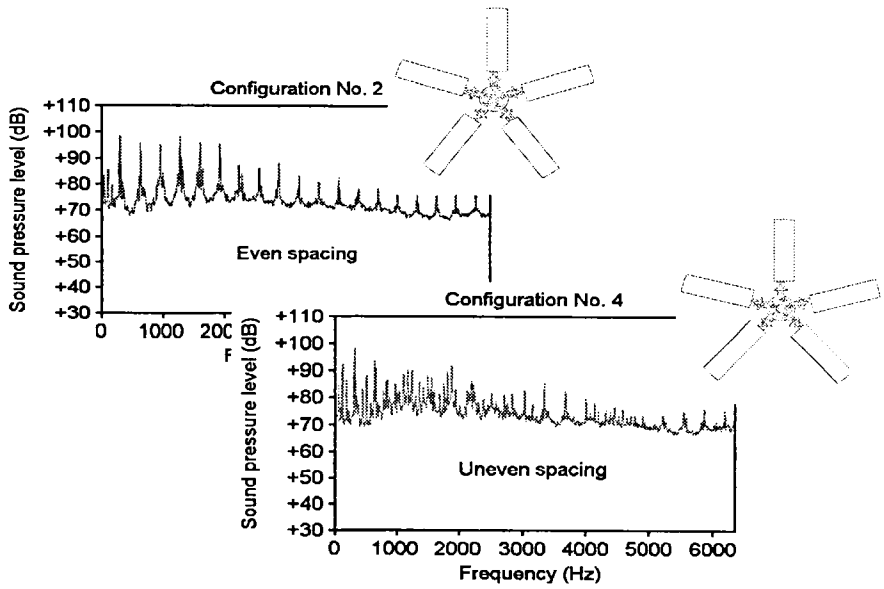

Figure 3-1. Modulated blade spacing - influence on acoustic spectrum

3.1.2 X-Force Control

BVI noise is generated when the vortices shed from the tips of main rotors are held in or near the plane of the rotor disk. When this occurs, the following blades pass near or through the shed vortices that are at least one revolution old. The resulting unsteady aerodynamic pressure gradient of the interaction results in a series of acoustic impulses emitted at the blade passage frequency.

The geometry of BVI is sketched in Figure 3-2. The side view shows the vertical distance between the blades and the wake. This illustrates the "miss distance," defined as the average vertical distance between the rotor disc and the shed vortices. BVI noise is strongly influenced by this miss distance. The effects of BVI are generally felt most strongly when the miss distance nears zero. In this situation, the vortices remain nearly in plane with the rotor and there is a greater chance of a strong interaction.

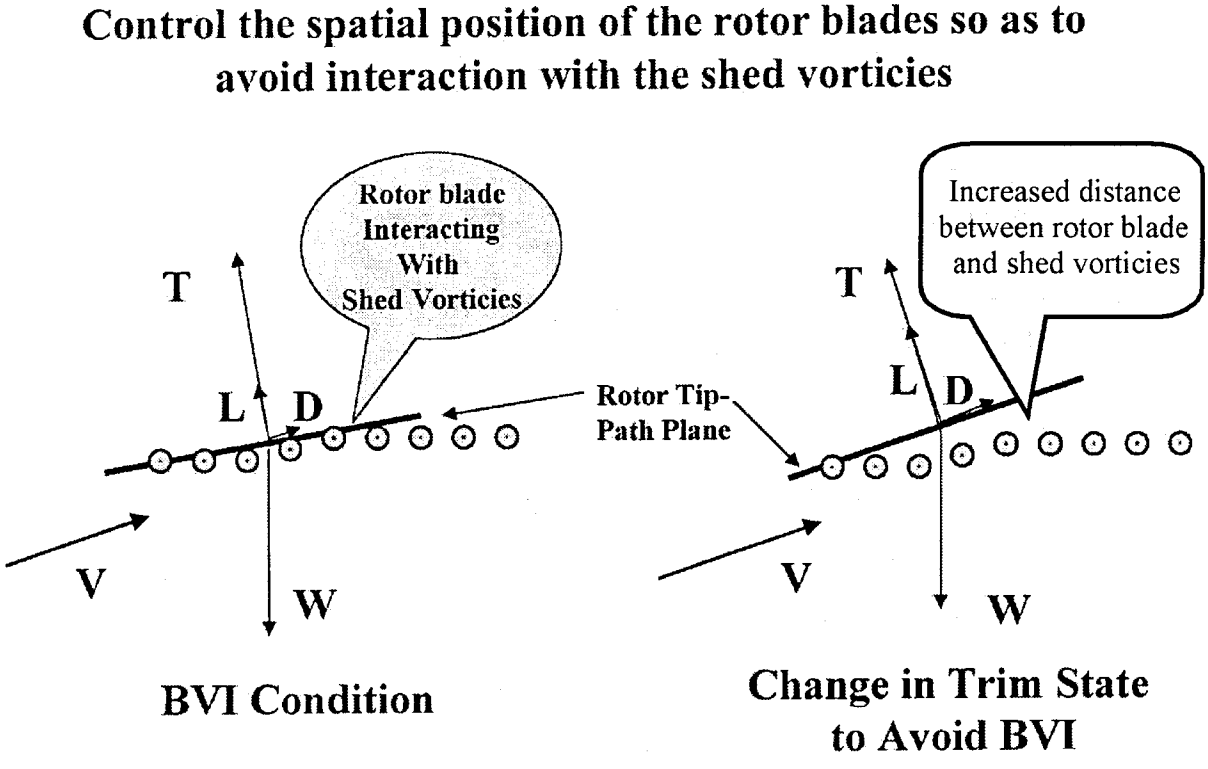

Figure 3-2. Side view of helicopter BVI geometry

By altering the force balance on the helicopter it is possible to control the miss distance between the vortices and the blades, and thereby control BVI noise radiation. Specifically, the addition

of x-forces (either propulsive forces or forces in the drag direction) to a helicopter tends to tilt the rotor plane, thus altering the miss distance. This has been shown theoretically (Reference 4) where novel methods of aerodynamically generating drag forces were investigated that tilt the tip-path-plane of the rotor forward. The additional forward tilt tends to move the wake farther from the rotor plane, increasing the miss distance as illustrated in Figure 3-2, thus mitigating or potentially preventing BVI.

The main research focus of *x-force control* has been to experimentally investigate whether it is possible to generate enough drag to significantly alter the geometry of the helicopter rotor force balance, thus reducing BVI while still maintaining reasonably steady flow with minimum buffeting. The goal of these experimental investigations has been to increase the baseline drag of the helicopter by 100% while assessing the additional moments, specifically pitching moment. This percentage increase in drag force has been shown to reduce BVI noise by as much as 12 dB SEL at the noisiest positions on the ground (Reference 5). The predicted noise with and without *x-force control* is shown in Figure 3-3, from this reference, for an approach angle of –3 degrees.

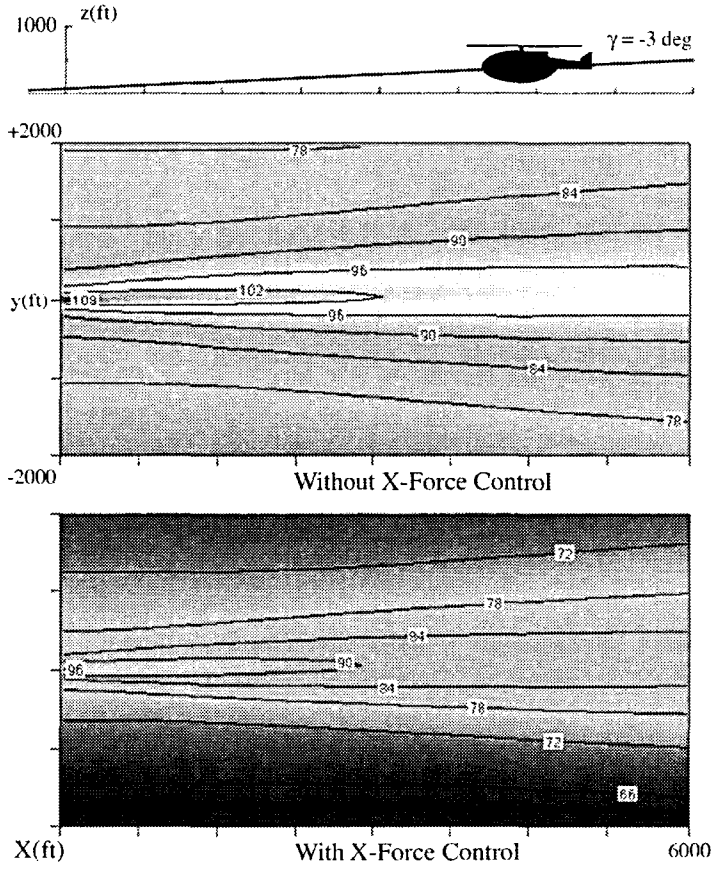

Figure 3-3. Predicted SEL ground noise with and without *x-force control* at -3 degrees approach angle

3.1.3 Reduced Tip Speed Design

Although not "revolutionary" or "innovative," tip speed reduction remains a powerful tool to lessen main rotor noise. However, experience has shown that there are finite, practical limits to the amount of tip speed reduction possible. These limits are established by the fundamentals of rotor design that must account for the acoustic contribution of all primary noise sources, particularly the anti-torque system, and for all inter-related disciplines, such as structures, performance, dynamics and controls.

Using these fundamentals, analyses have been made of main rotors designed to acoustically derived tip speeds. These analyses are described below, followed by discussions of the acoustic results and the impact assessment results. The latter includes limitations or penalties that would be incurred with the lower tipspeed designs, not only those directly associated with the rotor, but also any weight and cost penalties incurred in the drive train due to the increased torque.

3.1.3.1 Design Analyses

An initial analysis using a simplified approach was made in which a baseline turbine-powered helicopter's take-off gross weight was held constant and the useful load was allowed to vary. The baseline helicopter selected was configured with a single main rotor and conventional open tail rotor. The simplified approach minimized the number of variables that were allowed to change and provided a quantitative insight, in an isolated fashion, into the effects of tip speed variation on the noise and weight. However, a major limitation of this type of approach emerged: an inability to compare different levels of noise reduction for designs with equal productivity (long range cruise airspeed and payload-range).

To address this limitation, a point design analysis was conducted in which the baseline helicopter was modified to meet two specified noise reductions, 4 dB and 5 dB during an over-flight, while maintaining the long range cruise airspeed and payload-range capability of the baseline helicopter. Early on in this point design analysis, as expected, it became apparent that considerable modifications must be made to the tail rotor before the full acoustic benefits of reduced main rotor tip speeds can be realized. This is because the open tail rotor is a major contributor to the total noise in the vast majority of, if not all, turbine-powered helicopters. While modifications to the tail rotor will not be detailed here, their contributions to the total noise and their impacts on performance, weight, cost, etc. are taken into account in the point design analysis.

3.1.3.2 Acoustics Results

The acoustic results of the point design analysis are summarized in Figures 3-4 and 3-5 for 4 EPNdB and 5 EPNdB total noise reduction, respectively. In Figure 3-4, main and tail rotor

component noise levels are estimated for four candidate configurations and compared with those of the baseline helicopter. Similarly, Figure 3-5 presents estimates of component noise levels for three other candidate configurations. Tip speeds and cryptic descriptions of each candidate configuration are highlighted.

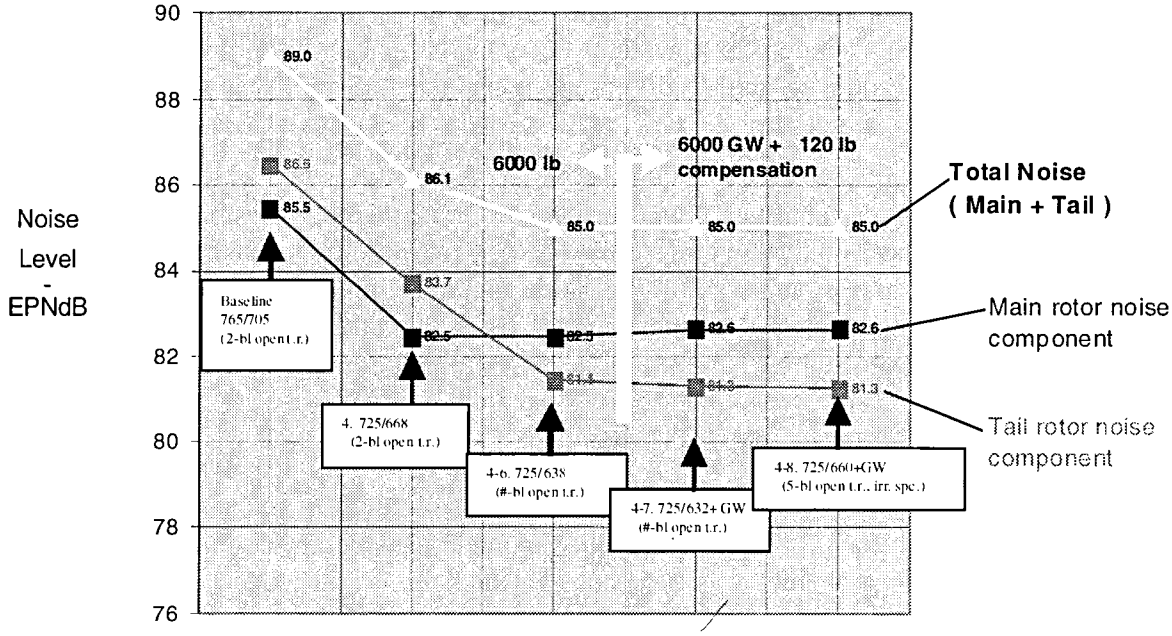

Figure 3-4. Estimated component noise levels for 4-EPNdB total noise reduction

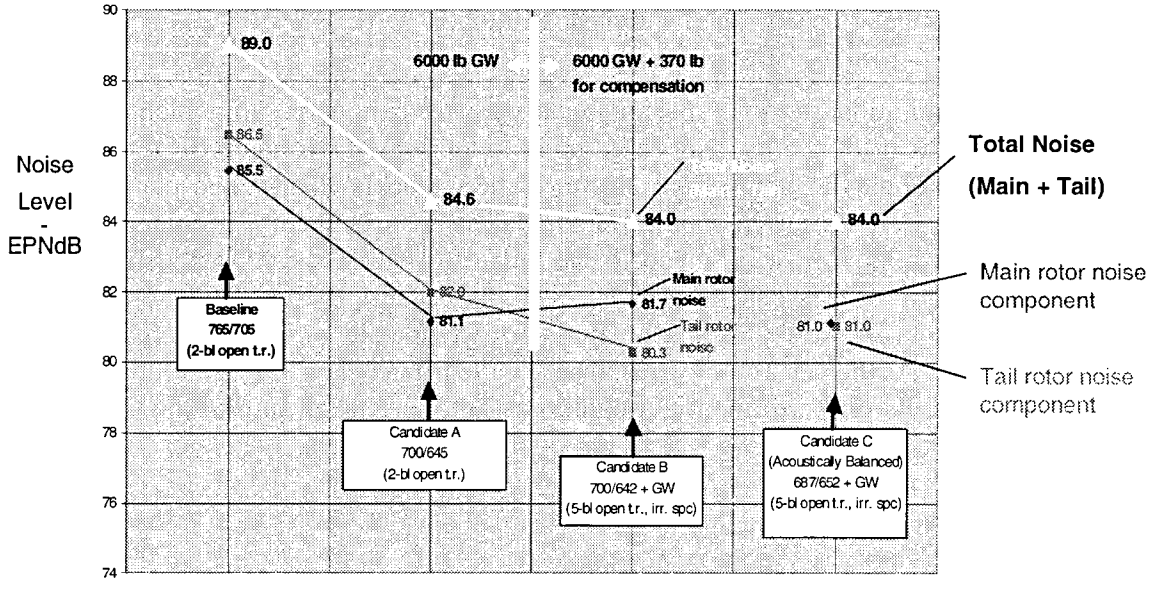

Figure 3-5. Estimated component noise levels for 5-EPNdB total noise reduction

Both sets of results show that reducing only main rotor tip speed has a limited effect on total noise. Hence, in the first candidate configuration of Figure 3-4, tip speeds of both the main and tail rotors are reduced, in this case by 5.5% each. Similarly, in the first configuration of Figure 3-5, tip speeds of the main and tail rotors are reduced by 9.3% each. Total noise level reductions of 3 EPNdB and 4 EPNdB are realized. Subsequent candidate configurations, in both figures, involve more extensive modifications to meet the total noise reduction targets of 4 EPNdB and 5 EPNdB.

3.1.3.3 Impact Assessment Results

The impact assessment results of the point design analysis are summarized in Table 3-1. The weight/torque/cost impacts are given for the candidate configuration, with reduced main rotor tip speeds, that meets the 5 dB over-flight noise reduction target.

Table 3-1. Weight/Torque/Cost Impacts

Rotorcraft Function	5 dB Over-Flight Noise Reduction Candidate
Main Rotor Tip Speed Decrease	9.3%
Gross Weight Increase	4.7%
Empty Weight Penalty	8.2%
Fuel Weight Penalty	1.2%
Main Rotor Torque Increase	15.6%
Non-Recurring Costs	$40.73m
Recurring Production Costs	$0.15m

As tip speed of the candidate configuration is decreased, the rotor solidity must be increased to maintain the long range cruise velocity and payload-range capability of the baseline helicopter. This in turn requires beefed up or added rotor control hardware. Tip speed reduction also increases the torque within the drive system, requiring beefed up drive train components and increased anti-torque capability. The impacts of these design modifications, along with related structural changes and a lower noise tail rotor, are reflected in the gross weight increase and in the empty weight-fuel weight penalties. These impacts cause the cost of producing the helicopter to go up, as illustrated by the higher non-recurring costs and the recurring production costs.

It can be seen from the point design analyses discussed above that reducing the tip speed of main rotors is an effective design tool to reduce helicopter noise levels. However, it cannot be done in isolation from changes to other noise sources and it typically necessitates substantial modifications of the entire drive system. As a result, weight penalties are incurred and costs increase to produce the modified helicopter.

3.1.4 Blade Tip Modification

Modification of the tip of main rotor blades has two potential payoffs: improved aerodynamics and reduced noise. Aerodynamic improvements include lower drag, delay of transonic flow, reduced tip loading, and less tip loss. The primary acoustic benefits include mitigating "de-localization" effects at high forward airspeeds, hence HSI noise, and diffusing the tip vortex which in turn lessens the interaction between blades and shed vortices, hence BVI noise.

Examples of blade tip modifications are illustrated in Figure 3-6. These include several aft swept configurations, a forward-aft double swept configuration, the BERP tip, and the Ogee tip. Most of these tips have been developed, tested and, in some cases, incorporated on helicopters for their aerodynamic improvements. In most instances, their acoustic benefits have also been assessed both at model-scale and full-scale; plus have been measured on whirl stands, in wind tunnels and in flight tests.

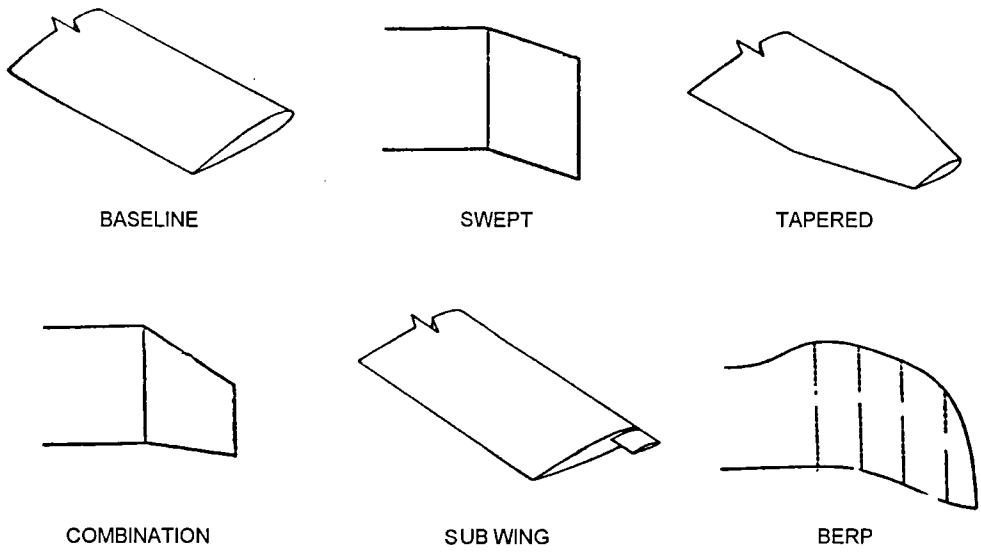

Figure 3-6. Examples of blade tip modifications

Two advanced tip shapes have been studied using Computational Fluid Dynamics (CFD) methods and wind tunnel studies. The tip shapes, a swept Ogee and a sub-wing design, are shown in Figure 3-7. The latter tip shape design involves a small secondary airfoil, or "sub-wing," attached to the tip of the rotor blade. The sub-wing generates a secondary vortex, slightly offset from the primary one. Interference between the two vortices tends to diffuse both very rapidly, mitigating the outcome of the blade-vortex interaction. Model studies using Schlieren visualization techniques have been made to refine the sub-wing design. Full-scale flight tests have also confirmed the effectiveness of such a design. These studies and tests have shown that

the tip vortex structure trailed from a blade can be significantly altered by adjusting the plan-form geometry.

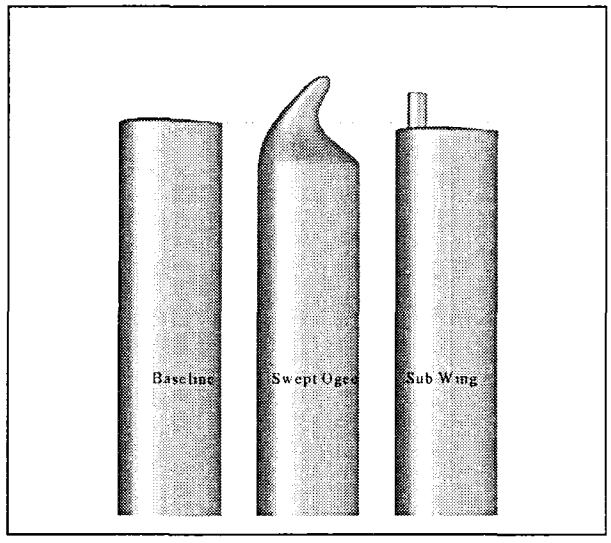

Figure 3-7. Blade tip modifications for BVI noise reduction

It is theorized that BVI noise reduction can be obtained for a rotorcraft in flight if the blade interacts with a diffuse vortex core instead of a concentrated vortex core. A typical computed flow for the sub-wing tip is shown in Figure 3-8. It is seen that the single vortex of the baseline tip is separated into two co-rotating vortices of approximately equal strength by the sub-wing tip. Both of the advanced tips were tested in conjunction with a baseline rectangular tip blade at the UTRC Main Wind Tunnel. Precise hot-film velocimeter data were generated at designated cross-sections of the wake for each tip shape at speeds up to a Mach number of 0.5.

Test results essentially confirmed the CFD predictions and showed that the trailing vorticity distribution could be tailored to a significant degree using plan-form variation. In addition to showing the redistribution of wake vorticity, test results also provided experimental confirmation of vortex conservation. That is, for the same lift, each blade tip shape produced the same net amount of trailing vorticity - only the distribution changed.

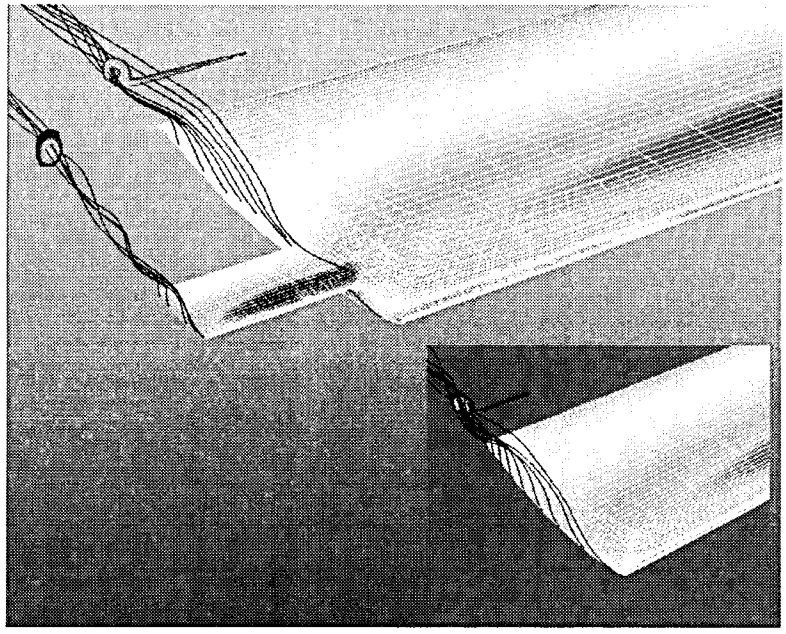

Figure 3-8. Comparison of computed flow fields for baseline and sub-wing tip blades

3.1.5 Airfoil Tailoring

Airfoil tailoring of rotor blades is a primary design means to improve performance and operating efficiency. For the most part, such tailoring results in beneficial acoustic effects. For example, thin airfoils at the blade tips delay the onset of shock stall, with its corresponding high drag, and mitigate HSI noise. Advanced high-lift airfoils improve climb performance, which in turn lowers the noise exposure during takeoffs. Such airfoils may have a downside, however, in that BVI noise may be intensified during descents. Studies continue to research airfoil types that retain the high-lift capability but react favorably, from acoustic standpoint, when in BVI conditions.

In the point design studies discussed in paragraph 3.1.3, airfoil types were selected for the different main rotor configurations that best met the reduced tip speed objectives. Their performance and acoustic effects were taken into account by analysis and design methods. These effects are detailed in paragraph 3.1.3.

3.1.6 Summary of Noise Reduction Concepts

In addition to the five noise reduction concepts discussed above in the preliminary assessment, active controls and variable diameter rotor were also considered. The advantages/disadvantages and risk/payoff of each of these technology concepts are summarized in Table 3-2.

Table 3-2. Summary of Noise Reduction Concepts

Technology	Advantages	Disadvantages	Risk/Payoff
Modulated Blade Spacing	Demonstrated to be effective on tail rotors; high potential for main rotors. Provides minimal impact on performance; potentially reduces vibration; improves sound quality; lessens perceptibility; potential aural detection benefits. Demonstrates advancement in the state-of-the-art (SOA).	Hub manufacturing more complex; increases cost.	LOW RISK HIGH PAYOFF
X-Force Control	Potential BVI reduction. Control in non-rotating system; deployable; drag increase demonstrated without undue buffeting and control issues. Likely applicable to tiltrotor aircraft.	Non-standard flight control.	MODERATE RISK HIGH PAYOFF
Reduced Tip Speed Design	Provides demonstrated reduction in all noise mechanisms. Point designs feasible that maintain airspeed and payload-range capabilities.	Will negatively impact weight and cost due to higher torque and correspondingly heavier drive system. Impact on vibration will be unique to each design. Anti-torque system must be extensively modified before reduced tip speed benefits can be realized.	LOW RISK HIGH PAYOFF
Blade Tip Modification	Demonstrated reduction in BVI and HSI noise. Passive shapes have potential to diffuse tip vortices, hence reduced BVI; relatively small weight increase. Active shapes offer potential BVI and HSI reduction; activated only when needed.	Impacts rotor design due to added centrifugal force; increases manufacturing costs. Actuator mechanism and logic for active shapes are complex. Potential increase in profile drag. Impact on vibration unknown, will be unique to each design.	PASSIVE: LOW RISK MODERATE PAYOFF ACTIVE; HIGH RISK MODERATE PAYOFF
Airfoil Tailoring	Reduces HSI noise; mitigates compressibility effects. Potential BVI reduction.	Somewhat higher manufacturing cost; possible profile drag increase. Complex actuator mechanism and logic, if active.	PASSIVE: LOW RISK MODERATE PAYOFF ACTIVE: HIGH RISK MODERATE PAYOFF
Active Controls	Potential BVI reduction; activation made in control system or on-blade; activated only when required.	Difficult to design and manufacture; potentially impacts blade structural integrity; probable vibration increase. Imposes penalty on component life or alternatively component sizing and reduced bearing life.	HIGH RISK MODERATE PAYOFF
Variable Diameter Rotor	Potential BVI reduction	Very complex, costly, and hard to implement. Not practical; penalties incurred throughout the flight envelope; useful only in certain flight segments.	HIGH RISK LOW PAYOFF

3.2 Most Promising Concepts - Detailed Design

All the noise reduction concepts listed in Table 3-2 are found to have advantages, either as reducing multiple noise mechanisms or just certain ones. Five of the seven concepts reduce or potentially reduce BVI noise. The disadvantages vary between concepts and involve added complexity, increased costs, higher weight and, for some of the high-risk concepts, more vibration and performance penalties. Concepts with the lowest risk and highest payoff include *modulated blade spacing*, reduced tip speed, and *x-force control*. These are considered the most promising concepts to take to a detailed design stage as described in the following paragraphs.

3.2.1 Modulated Blade Spacing

The advantages of the *modulated blade spacing* concept are many: it has minimal impact on performance and potentially reduces vibration; it reduces sound levels and improves sound quality when incorporated on tail rotors; it lessens perceptibility; and it potentially has aural detection benefits. It is believed that the lower source frequencies associated with a main rotor can be altered similarly to those of a tail rotor, resulting in the advantages noted above. The preliminary assessment of this concept indicates that a main rotor incorporating *modulated blade spacing,* while presenting a challenge to the current library of analytical techniques, can certainly be designed, built and tested at model scale. Also, no obvious barriers exist which would make a full-scale flight version impractical.

3.2.1.1 Ground Rules for Concept Evaluation

In the evaluation of the *modulated blade spacing* concept, several ground rules have been established and followed. First, the rotor design incorporating *modulated blade spacing* must consider three aspects: acoustic design, aerodynamic design, and production feasibility. Second, an acoustic analysis must be performed in two parts: a noise-prediction validation study in which modifications, unique to *modulated blade spacing*, to current analytical techniques are made; followed by a specific analysis of the reduced noise configuration using the modified analytical techniques.

3.2.1.2 Rotor Design

The approach taken to design a main rotor incorporating *modulated blade spacing* departs from that typically followed for conventional rotors. First of all, the basic configuration is designed from an acoustic standpoint, namely to meet the study's noise reduction targets. Next, the aerodynamic design of the reduced noise configuration is performed such that the performance closely matches that of a selected baseline rotor. Finally, a determination is made of the feasibility to produce the reduced noise configuration.

3.2.1.2.1 Acoustic Design

Two efforts are described to design a main rotor from an acoustic standpoint: an analytical assessment of different blade spacing configurations and the development of audio simulation methodology. In the first effort, five candidate blade spacing configurations were generated representing percentage modulations of 5%, 7.7%, 10%, 12% and 15%. The latter effort makes it possible to generate audio wave files based on user specified percent modulation spacing and then hear an audio simulation of that configuration. This capability provides an automated means to generate audio wave files for various design candidates and conduct sound quality assessments of each - a needed and intriguing follow-on study.

The reduced noise/improved sound quality rotor design is based on the principle of sinusoidal modulation. The idea is to employ uneven blade spacing, using a sinusoidal varying pattern, to redistribute the tonal content of the rotor noise across the audible spectrum. The basis for this concept emanates from the subjective observation that annoyance from rotor noise harmonics is related to the tone-to-broadband noise ratio. The goal of this type of spacing is to redistribute the harmonic energy by generating a number of side-bands for each harmonic. This in turn reduces the amplitude of each harmonic and produces a "broadband-like" spectrum.

For a sinusoidal modulated design, the angular positions of the modulated rotor blades relative to evenly spaced blades are determined by a sinusoidal function. The equation used here to determine a specified percentage of blade spacing change is

$$\phi_i = \theta_i + b \sin (2\,\theta_i)$$

Where,

θ_i = angular position of the i the non-modulated blade

ϕ_i = angular position of the i the modulated blade

b = modulation parameter

Using a computer program that employs the above equation, design candidates were generated for various percent modulations: 5%, 7.7%, 10%, 12%, and 15%. A second program was used to perform a Fourier Series analysis of each design candidate.

The results of this analysis are shown in the five spectral plots of Figure 3-9. Each plot demonstrates the potential reduction in harmonic level relative to an evenly spaced rotor. For example, it can be seen that there is a noticeable "notch" in the spectrum at the 35th harmonic for

the 5% spacing case. This "notch" shifts toward lower harmonics with increasing percent modulation up to 10% spacing, where a second "notch" appears and continues the trend.

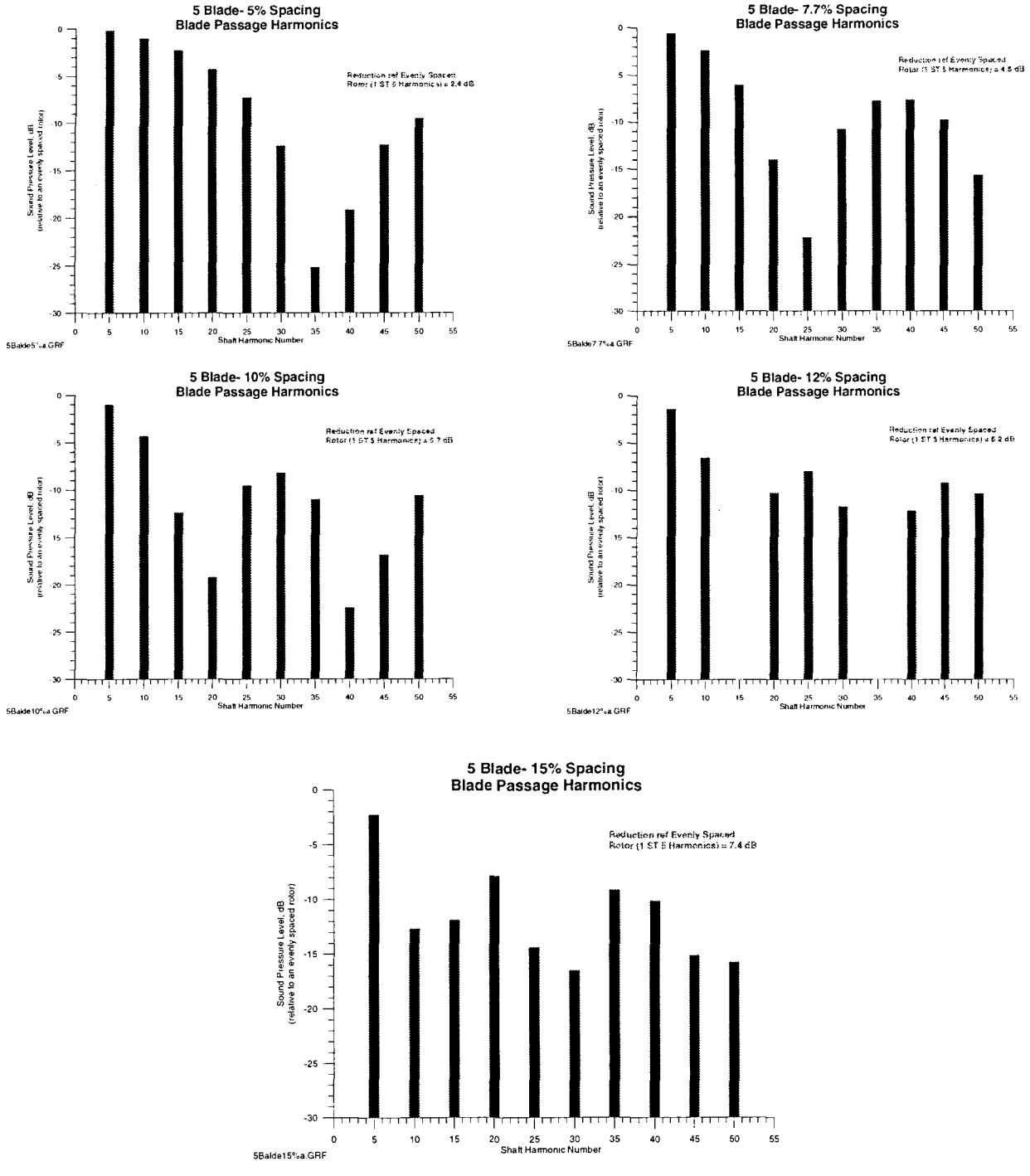

Figure 3-9. Analytical assessment of candidate 5 blade designs

For each of the percentage spacing cases in Figure 3-9, the harmonic levels are summed and then subtracted from the even spaced blade case to obtain the total harmonic reduction. This is shown in Figure 3-10. This assessment indicates that higher percent modulations offer greater reduction in harmonic levels.

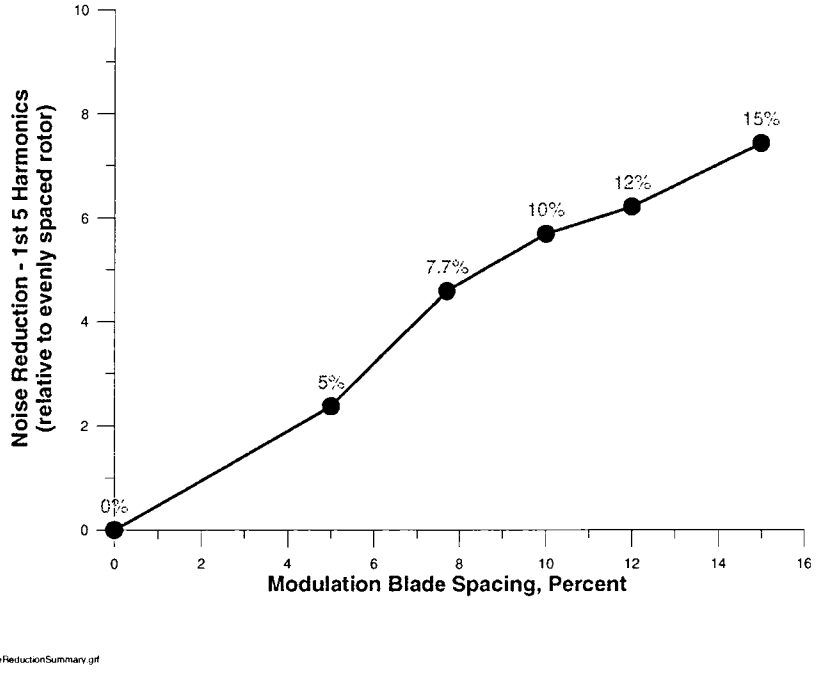

Figure 3-10. Effect of *modulated blade spacing* on 1ST 5 harmonics

In addition to analyzing the amount of harmonic noise reduction possible with modulated blade spacing, it was determined that an assessment of the future rotor's sound quality should be a factor in the overall design. Sound quality considers not only the loudness of a source but its frequency and time dependent characteristics, and how humans perceive it. Several industries, e.g., the automotive companies, have capitalized on the concept of sound quality to design transportation vehicles with interior and exterior sounds that are more pleasing to customers. In like manner it is important to design future helicopter rotor systems that consider sound quality.

To assess a rotor's sound quality, an audio simulation methodology was developed. Appendix A describes in detail this methodology. It utilizes a noise recording of a helicopter flyover from which a baseline acoustic waveform is replicated and spliced together to represent a complete rotor revolution. The angular spacing between blades is modeled by proportionately spacing the waveforms. The end result is an automated simulation of the sound of any rotor configuration being designed.

3.2.1.2.2 Aerodynamic Design

A study was undertaken to design a SILENT rotor configuration in which the performance would closely match that of the baseline rotor. The study's aim was to minimize the penalty on the helicopter's payload-range capability. Details of the aerodynamic design are presented in Appendix B. The assumptions used to assess the payload-range capability are listed, the configurations evaluated are described, and payload-range comparisons are presented of the baseline and four SILENT rotor candidate configurations. Also, a plan-form view is given of the SILENT rotor configuration selected and its basic aerodynamic properties.

The selected SILENT rotor configuration consists of five blades, a tip speed of 665 feet per second, a thrust-weighted chord of 12 inches, and a radius of 19.5 feet. It includes the reduced noise features of *modulated blade spacing* and swept ogee tip shape. For comparison, the baseline rotor consists of four blades, a tip speed of 765 feet per second, a thrust-weighted chord of 10.6 inches, and a radius of 18.5 feet. There is a payload penalty for the SILENT rotor configuration of 162 pounds. This equates to one less seat filled, out of eight, when the SILENT rotor is installed on the baseline helicopter.

The SILENT main rotor configuration is sketched in Figure 3-11.

5bld427d

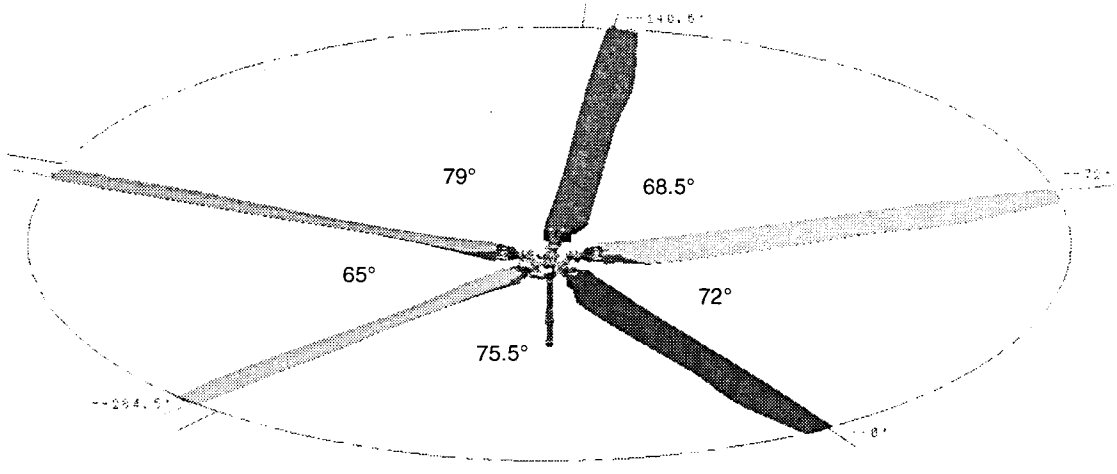

Figure 3-11. Sketch of SILENT main rotor configuration

3.2.1.2.3 Production Feasibility

The SILENT main rotor configuration can be readily produced using current manufacturing techniques and practices. Manufacturing the hub is more complex and costly due to the uneven spacing between the blades, but metal forging or composite filament winding technology can easily accommodate the added complexity. There is sufficient space between blades for conventional rotating controls, so no hurdles in this regard are foreseen. Manufacturing the modified blade tip is also more complex and costly. However, the swept ogee tip shape does not depart that much from other tip shapes currently being incorporated in production composite blades.

From the standpoint of dynamics, the SILENT main rotor presents a unique challenge since the uneven blade spacing creates multiple excitation frequencies. The analysis program COPTER has been used to evaluate the hub pitching moments and the shear forces. It is shown that avoiding structural responses to all the excitation frequencies is unlikely. Hence, active isolation mounting is deemed necessary so that the amplitude of the excitation can be controlled in a manageable way. As a result, it appears that such an active isolation system would be essential in any full-scale application of the SILENT main rotor

3.2.1.3 Acoustic Analysis

The rotor geometric parameters for the baseline 427 main rotor and the SILENT main rotor were modeled analytically for inclusion in WOPWOP (Reference 6). For each blade, the radial properties (chord, thickness, twist) were curve fit and included in the FUNE2 subroutine of WOPWOP. The chordwise thickness and camber distribution was also determined from the discrete airfoil section data and modeled analytically for each airfoil section along the radius of the blade in subroutine FUNE2Q. Thus WOPWOP utilized a mathematical description of the blade for all the noise computations. All measurements for WOPWOP were converted to metric units. To ensure that the blade coordinates were input properly, a modification to WOPWOP was made which output the surface grid used by WOPWOP in the numerical integration. The blade geometry was verified visually to correspond to the geometrical information of each blade.

Blade flapping, collective and cyclic pitch were included in the WOPWOP noise predictions. Only the constant and first harmonics of these motions were included. No lead-lag motion was modeled for these predictions. The forward shaft tilt of the rotor was input into WOPWOP to account for the orientation of the rotor in each of the cases. Although WOPWOP is unable to accommodate lateral mast tilt, the 427 rotor system's net lateral (left) mast tilt of 0.94 degrees was included by adjusting the positions of the microphone locations on the ground.

The section lift and drag from COPTER calculations was provided in the form of an MS Excel spreadsheet. The spreadsheet was modified slightly so that it could be read by WOPWOP at the beginning of each case. In WOPWOP, the forces were converted to metric units and the time

derivatives of section forces were computed using the standard 2nd –order central difference finite difference approximation. Both section forces and the time-derivatives of section forces were interpolated first in the radial direction and later in the chordwise direction in the process of the noise prediction in WOPWOP. Linear interpolation was used in each interpolation of the data (i.e., radial, chordwise, and azimuthal). The section force data was given with an azimuthal resolution of one degree. The data was assumed to be periodic for the acoustic predictions—therefore only one rotor revolution was needed. Linear interpolation was also used for the azimuthal interpolation needed to provide blade loads at the retarded time of the center of each surface element in the numerical integration.

The section forces were assume to act at the quarter chord of each radial station along the blade. A compact chordwise model for the load (Reference 7) was utilized for this work. In this model, the compact chordwise loading is simulated in WOPWOP with a triangular loading distribution in the chordwise direction extending from 5% before to 5% after the quarter chord location. The peak amplitude of the loading is chosen such that the integral of the triangular loading gives the correct section lift and drag with integrated. Although section drag is often neglected in computations of this type, both lift and drag forces were used in all of the present WOPWOP noise predictions.

3.2.1.3.1 Noise Prediction Validation Study

Several modifications to the standard version of WOPWOP were required to model the unique aspects of the SILENT rotor. These modifications are described below, followed by an explanation of the operating conditions and some details of the noise predictions themselves.

Two types of modifications to WOPWOP were required. The first modification required was to enable long observer time runs (typically 10-30 seconds of observer time). The standard version of WOPWOP only allows up to 1024 points in the acoustic-pressure time history. While this is appropriate for cases that include up to a few rotor revolutions, it was not sufficient for the predictions of an entire overflight required for this task. The needed modifications were relatively minor–they consisted mainly of increasing array sizes and modifying the algorithm for updating the observer time and position. For a 30 second segment of observer time, as many as 135,000 points were computed in the acoustic pressure time history (nominally 128 points per blade passage period).

The second modification to WOPWOP–enabling modulated rotor blade spacing–was more extensive. WOPWOP was modified to allow user input of the angles between the blades. In the standard version of WOPWOP the angle between the blades is assumed to be constant. In the modified version of WOPWOP, the angles are input by the user instead. Another aspect of modulated blade spacing is that the loading on each of the blade may be different from the others at a give azimuth angle. Therefore, WOPWOP was also modified so that each blade would utilize a unique loading dataset. To implement this feature, the code added a global variable to keep track of which blade was currently generating the noise. Then the input

subroutine FUNPSI was enhanced to use the correct loading from the current blade. The blade flapping and pitch angles, which are functions of azimuth, were assumed to be the same functions of azimuth for ah all the blades. The updated version of WOPWOP was tested thoroughly to ensure that results for a rotor with equal blade spacing were identical to the standard version of WOPWOP.

For the long runs specified in this analysis, it is impractical to use the acoustic pressure time history directly to characterize the noise or make comparisons between the noise of different rotors. Hence, the WOPWOP acoustic pressure time histories were post processed. The post-processing consisted of applying a Hanning window to each one-half second interval of the discrete acoustic pressure time history. A Fourier transform was then performed on each half second interval and the Overall Sound Pressure Level (OASPL) and the A-Weighted Sound Pressure Level (SPL_A) were computed for the interval. A "slow-time weighting" of the form

$$L_{slow}(k) = 10\ln\left[0.13\times10^{0.1L(k-3)} + 0.21\times10^{0.1L(k-2)} + 0.27\times10^{0.1L(k-1)} + 0.39\times10^{0.1L(k)}\right]$$

effectively takes the SPL levels at four different times and smoothes the time history of SPL. This is approximately equivalent to what is done during certification flight testing, however, in that case each third-octave band is "slow-time weighted" rather than the integrated SPL metric (OASPL or SPL_A). The "slow-time weighted" SPL value is plotted versus the time corresponding to interval k, which is the center of the last of the four half-second intervals.

It should be noted that A-weighted SPL levels are significantly lower than measure in the flight test data. The reason for this has not been explored in much detail, but there are some things to consider. First, the processing of the discrete frequency noise is significantly different than is actually done in the flight test. In the flight test third-octave data is analyzed with the slow-time weighting function rather than an integrated level. Furthermore, the flight data has several high frequency noise sources that are not account for here – engine noise, tail rotor noise, broadband noise, etc. Finally, it was noticed in the data processing that the predicted levels are very close to flight data when the Hanning window is not applied to the time history data before the Fourier transform. The trends did not change, only the absolute level. For this reason no direct comparison with flight data is made, but it is still expected that the relative comparison between rotors – which is completely consistent – reflects an accurate qualitative and quantitative comparison.

3.2.1.3.2 Analysis of SILENT Rotor

The prediction of acoustic pressure was performed at three microphone locations, for each of three flight conditions (flyover, take off, and approach). Three separate rotor configurations were evaluated: a) the 427 main rotor (baseline); b) 5-bladed SILENT rotor with equal blade spacing; and c) 5-bladed SILENT rotor with modulated blade spacing. The three microphone locations utilized are the microphone locations required in noise certification. Microphone #1 is

150 meters on the left (port) side of the aircraft, microphone #2 is below aircraft centerline and microphone #3 is 150 meter on the right (starboard) side of the aircraft. For convenience in the WOPWOP predictions, a time t=0 was chosen to be when the helicopter was directly overhead (over microphone #2). In the data files and in the time-history plots, values of time where t<0 are prior to the helicopter flying directly overhead and times t>0 are after the aircraft has already passed overhead. At time t=0, the aircraft was specified to be 150 meters above microphone #2 for both the flyover and takeoff conditions, while for the approach condition the aircraft was only 120 meters above microphone 2 at t=0. The three flight conditions evaluated are shown in the table below. For each of the flight conditions, the velocity is assumed to be constant throughout the duration of the flight.

Table 3-3. Evaluated Flight Conditions

	Airspeed (m/s)	Ascent Angle (deg)	Nominal Height at t=0 (m)
Flyover	58.65	0.0	150
Take Off	32.05	18.2	150
Approach	30.66	-6.0	120

The predicted OASPL is plotted as a function of time for each of the three rotors at each of the three microphone positions for the flyover flight condition in Figure 3-12. For the flyover condition, the noise prediction began approximately 30 seconds before the helicopter is directly overhead and ended approximately 10 seconds after the helicopter has passed. The peak noise occurs slightly before the helicopter is overhead for each of the three rotors.

The OASPL level shows that all three rotors have similar maximum levels at all microphone locations, but the 427 rotor seems to have higher OASPL levels before the peak level occurs. This is probably due to a higher thickness noise level caused by the higher rotor-tip speed of the 427 rotor.

In contrast, the A-weighted SPL is plotted versus time for each of the three rotors and three microphone positions in Figure 3-13. In this figure, both SILENT rotor configurations have significantly lower noise levels at all times – from approximately 12 dBA lower at t = -30 seconds to at least 4 dBA when the helicopter is overhead (depending upon the microphone location). The comparison between the even and modulated rotor spacing for the SILENT rotor is more subtle, but the modulated blade spacing seems to be quieter by approximately 2 dBA for microphone 2 and 3, yet has a higher peak noise than the evenly spaced rotor just before time t=0.

Figures 3-14 and 3-15 show the OASPL and A-weighted SPL for the take-off flight condition. For this flight condition the evenly spaced SILENT rotor seems to be superior both for the OASPL and A-weighted levels. The modulated SILENT rotor seems to have similar dBA noise reductions, but is not quite as good for the OASPL at any of the microphone locations. One notable feature is that A-weighted SPL levels for all three rotors are nearly the same for microphones 2 and 3 for a brief period at approximately t=0. The predicted acoustic pressure

time history, which contains the thickness and loading noise as separate components, is available for more in depth analysis and understanding of these results.

Finally, in Figures 3-16 and 3-17, the OASPL and A-weighted SPL time histories are plotted for the approach condition. Here the results are mixed and some careful analysis is needed to determine the advantages of the SILENT rotors. In general, the evenly spaced SILENT rotor seems to produce a lower A-weighted SPL after t=0 while the modulated SILENT rotor had significantly lower dBA levels before t=0.

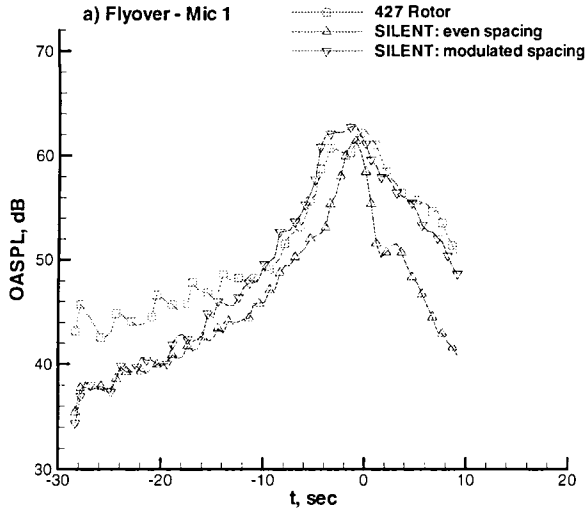

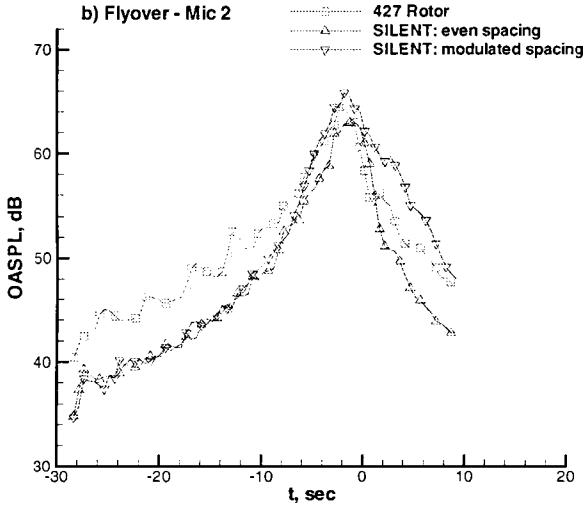

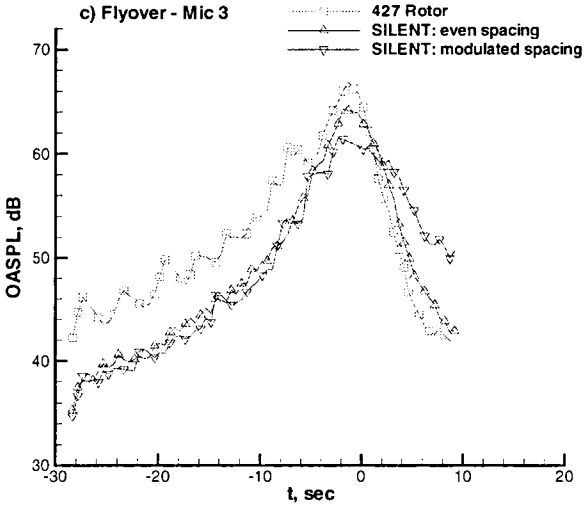

Figure 3-12. Overall sound pressure level time history for the flyover condition

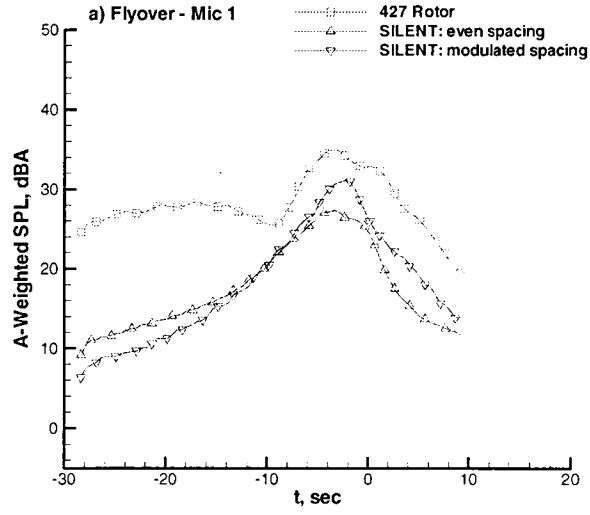

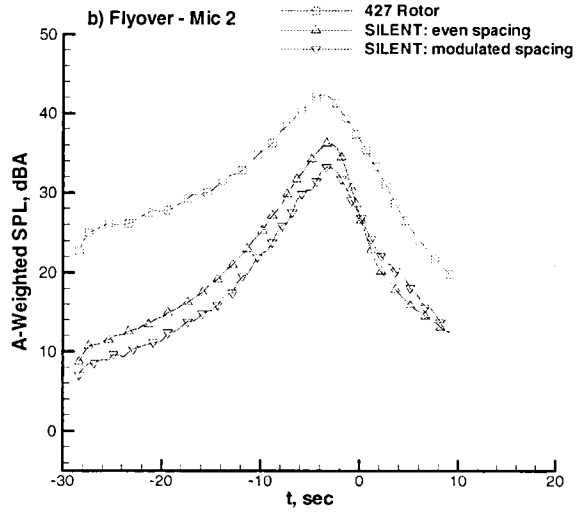

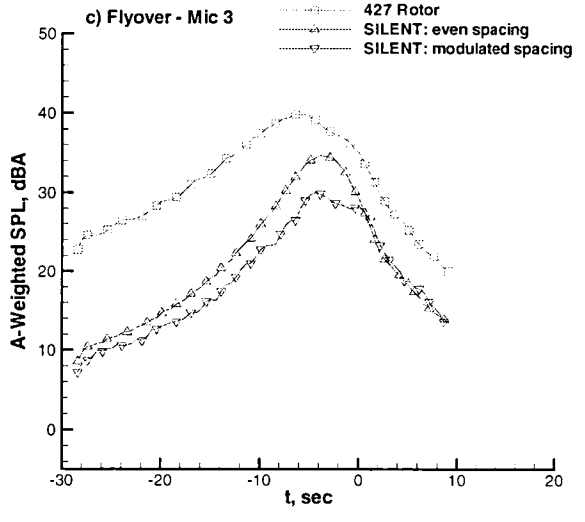

Figure 3-13. A-weighted sound pressure level time history for the flyover condition

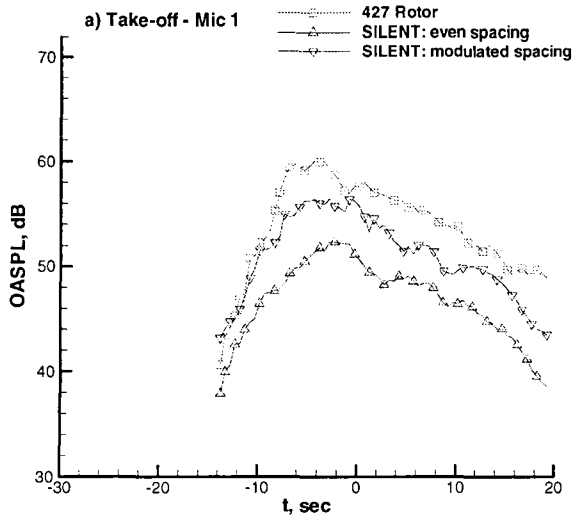

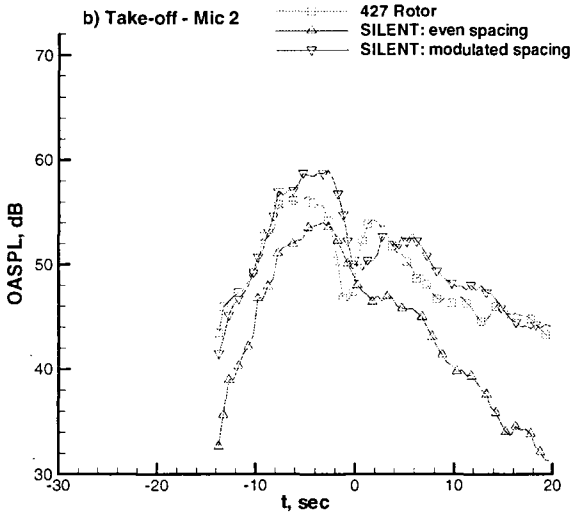

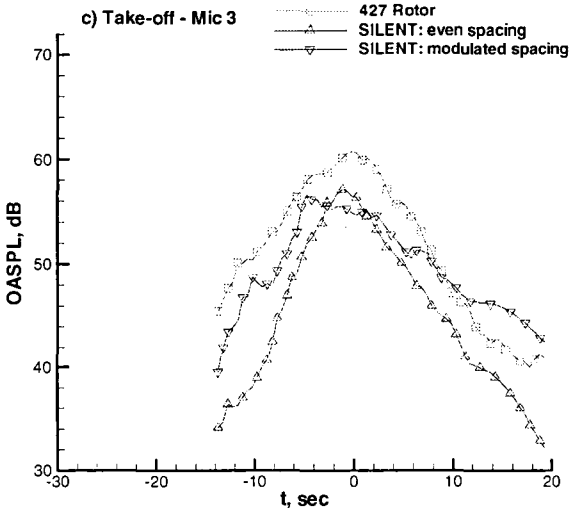

Figure 3-14. Overall sound pressure level time history for the take-off condition

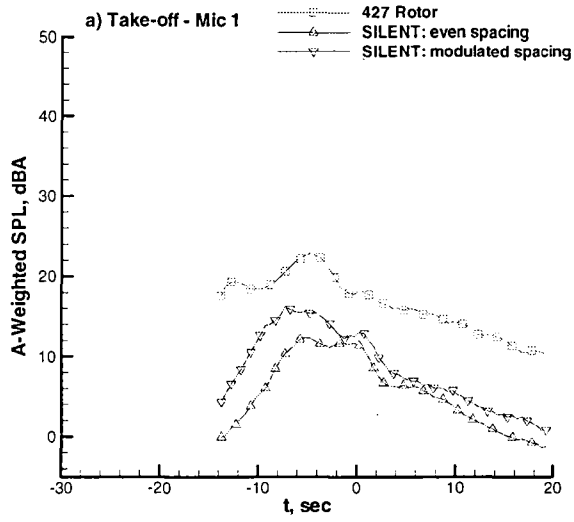

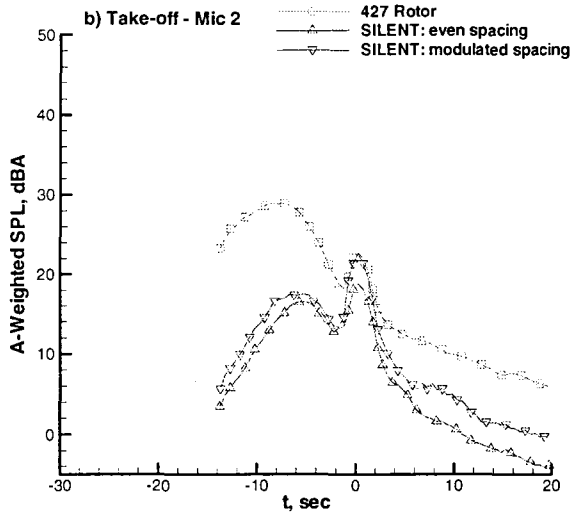

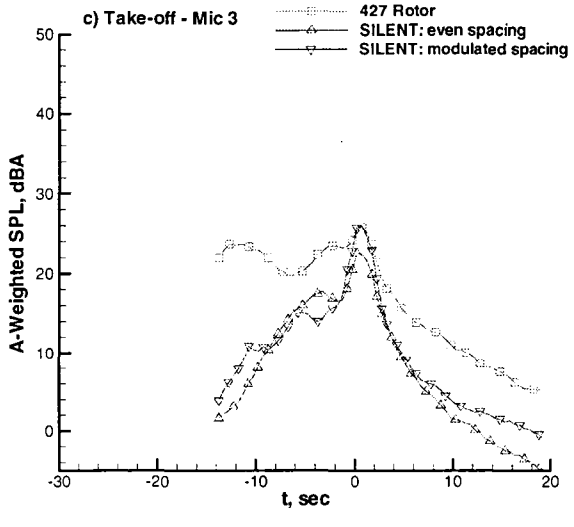

Figure 3-15. A-weighted sound pressure level time history for the take-off condition

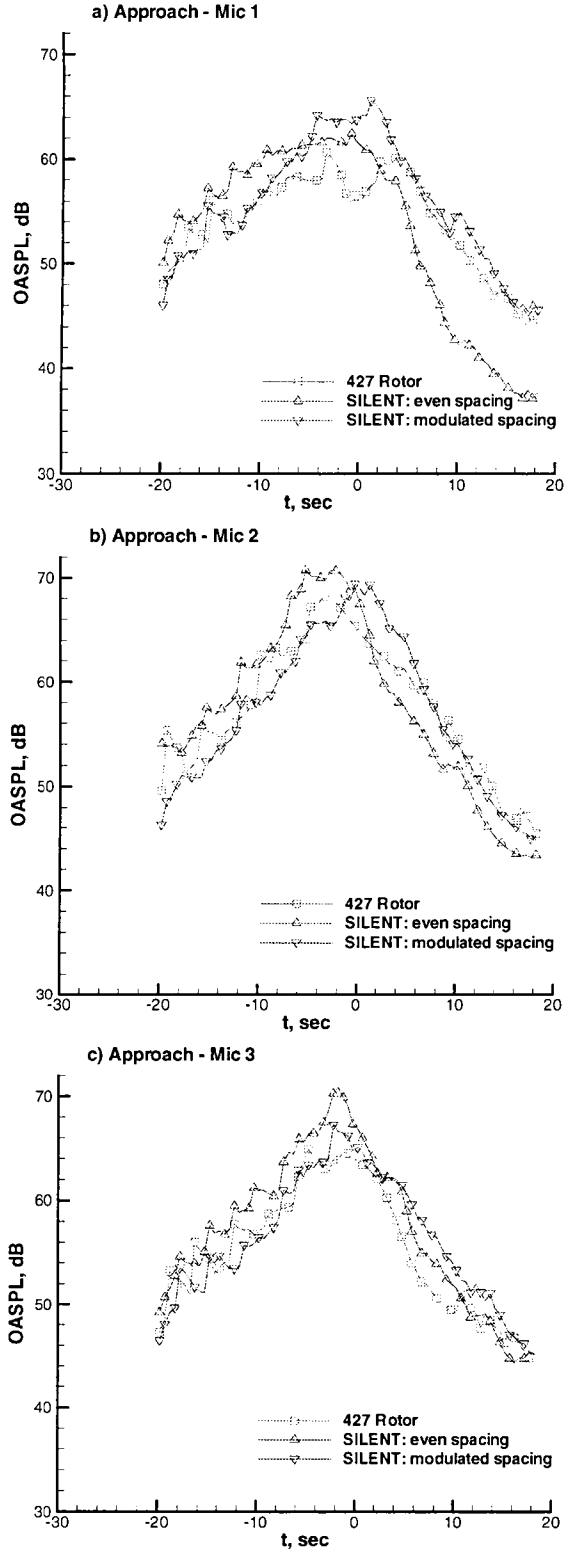

Figure 3-16. Overall sound pressure level time history during the approach condition

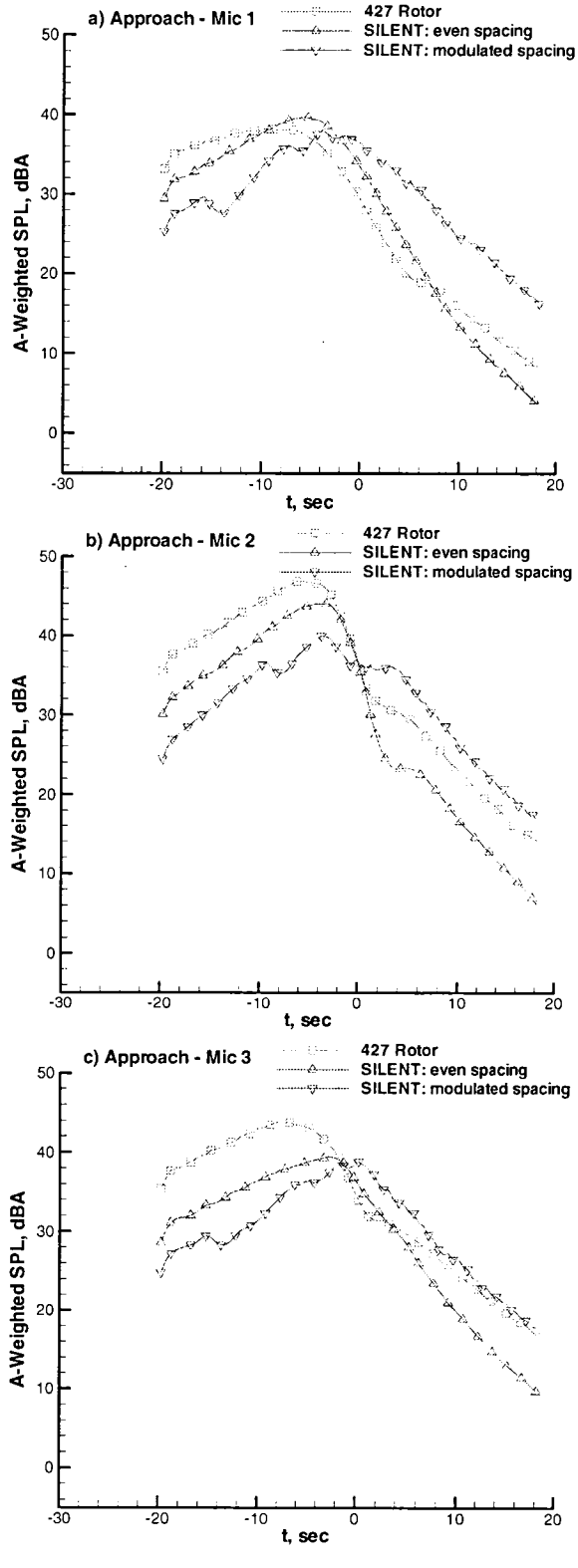

Figure 3-17. A-weighted sound pressure level time history during the approach

Two considerations should be made when evaluating these predictions. First, the operating conditions for the SILENT rotor seemed to have more BVI that for the 427 rotor. Thus the particular choice of conditions may have not shown the true noise reduction capability of the two SILENT rotors. Secondly, the character of the modulated rotor acoustic pressure time history is strikingly different from the evenly spaced SILENT rotor, and the 427 rotor for that matter. A short time history taken from the flyover condition at t=0 is shown in Figure 3-18. Notice that for this short time duration, amplitude of the modulated rotor is quite different from the other rotors. Many other examples can be found by looking at the time history predictions.

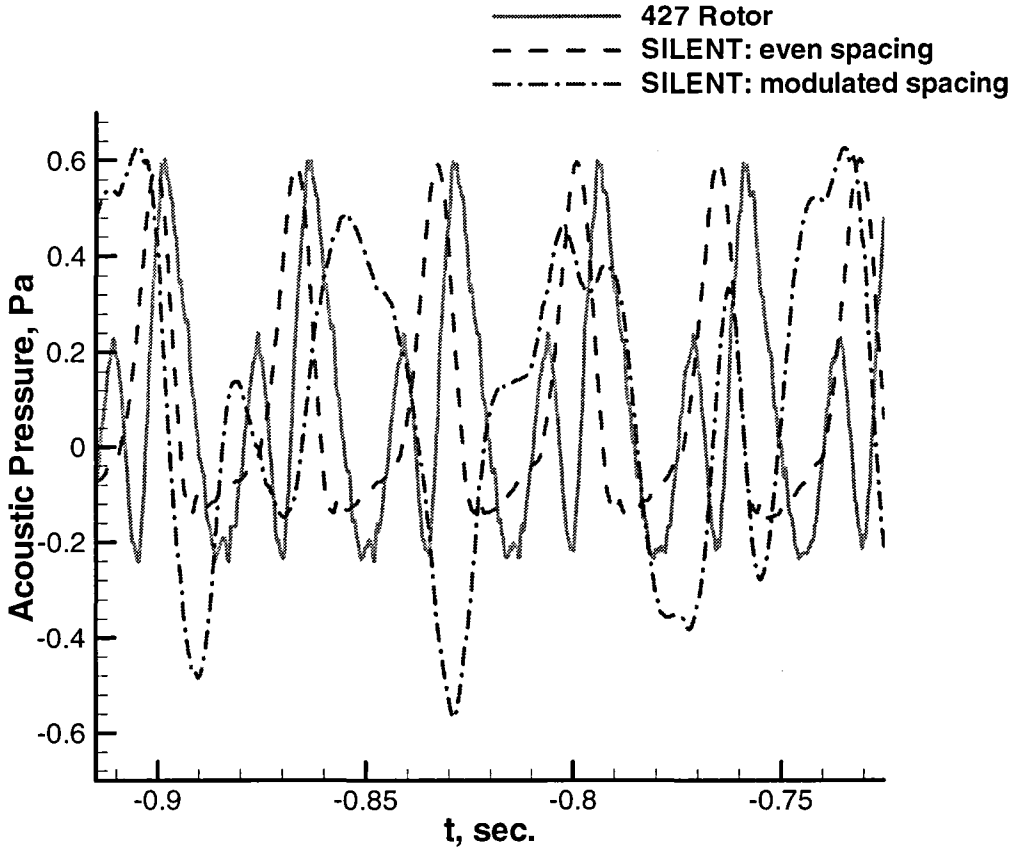

Figure 3-18. Comparison of acoustic pressure time history for approximately one rotor revolution

Post processing of the computed acoustic pressure time history was performed to provide computer files suitable for audio playback. These files are described in Appendix C. A CD-

Rom disk has been produced with the full acoustic pressure time history of each computation. Together with the audio playback files, this disk is also described in Appendix C.

3.2.2 X-Force Control

Flight path control has been shown to be an effective means of avoiding blade vortex interaction and its impulsive acoustic emission. The general combinations of airspeed and descent rate that produce BVI noise have been documented experimentally. This has lead to the *x-force control* design concept that mimics those flight controls used to reduce BVI noise. In such a design, the force balance on the helicopter is controlled, thereby avoiding or at least minimizing BVI.

3.2.2.1 Description of Drag Devices

In developing this promising design concept, tests have been conducted of multiple types of drag devices placed on and around a scale model helicopter fuselage. During testing, all forces and moments were monitored to determine the potential impacts of the drag devices on aspects of the helicopter's flight moment balance. Since the tests were carried out only on a fuselage, the expectation of somewhat more than 100% increase in fuselage drag was necessary to replicate the increase of overall drag of the helicopter.

Four drag devices were tested on the scale model helicopter fuselage as seen in Figure 3-19. The first device investigated was a cone on a boom aft of the tail of the fuselage, as shown in Figure 3-20. The cone was on a 10-inch boom from the rearmost point of the fuselage so that it could, if scaled up, clear any tail rotor. The cone itself was 1.04 feet deep and had a 60° angle.

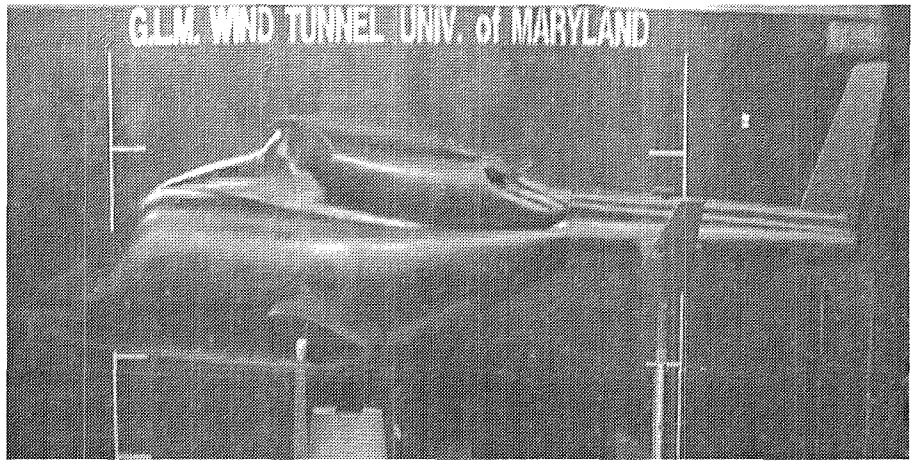

Figure 3-19. Scale model helicopter fuselage

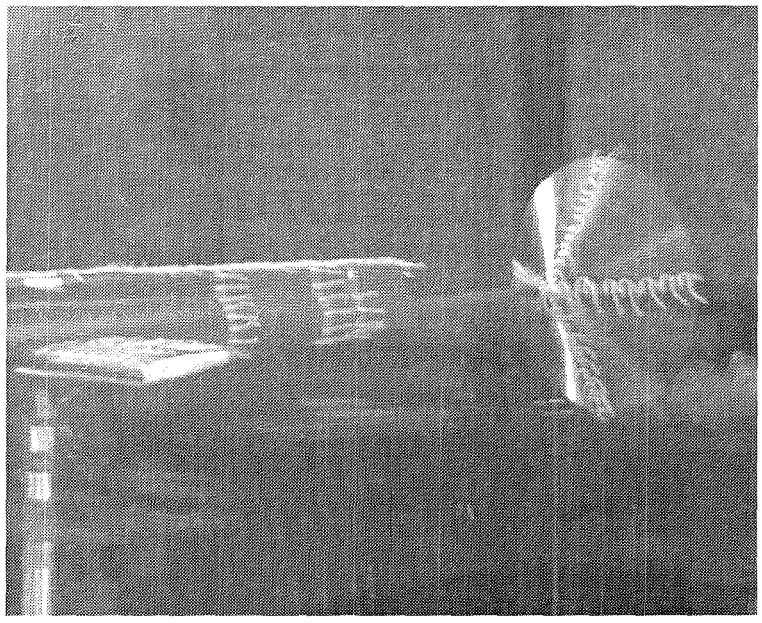

Figure 3-20. Cone connected to tail boom

The second device was a split flap simulator composed of two arrays of 6 flat strips (each 6-inch long by 1-inch wide) separated from each other by 0.25-inch above either fairing as shown in Figure 3-21. The third device was a single long flat plate (24-inch long by 3-inch tall) that was placed underneath the fuselage as seen in Figure 3-22. This was designed to simulate a plate that could be deployed with the landing gear during descents.

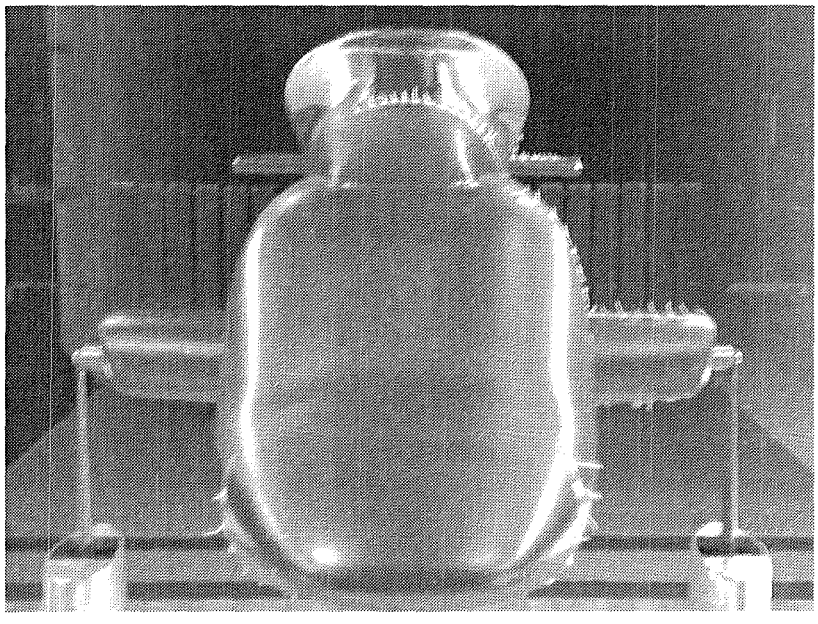

Figure 3-21. Split flap simulator

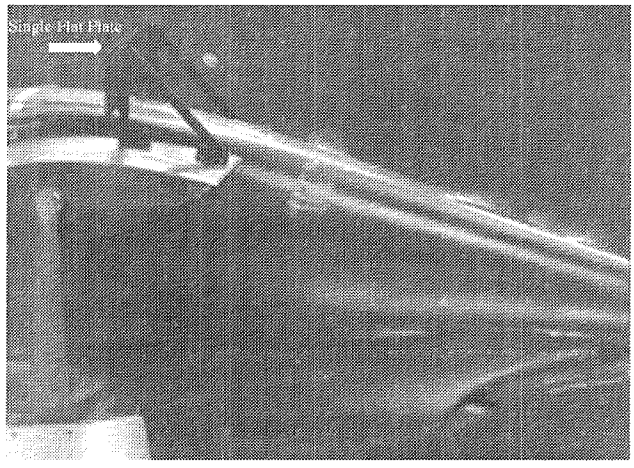

Figure 3-22. Flat plate under fuselage (Note: fuselage inverted)

Micro-drag generator (MDG) strips and rings were the fourth drag device tested. They were used in many different configurations, being placed under and around the fuselage as illustrated in Figures 3-23 and 3-24. The MDG devices were angle brackets 0.5-inch high, segmented so that they could be wrapped around the curving fuselage. The final total linear length of these devices was 134.4-inch. A planned fifth device using solid drag brake simulators, where flaps would be on the fairings, was eliminated from the test when it was observed that the split flap had a disproportionately large impact on the flow, and caused unacceptable buffeting of the model during the test.

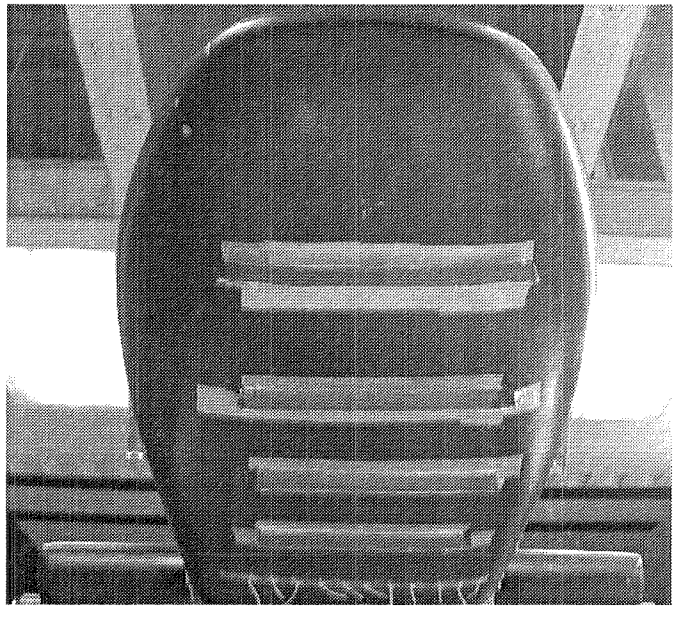

Figure 3-23. Micro-drag generator (MDG) strips

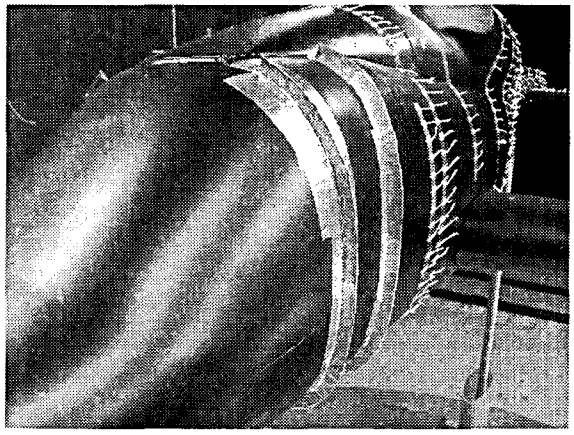

Figure 3-24. Micro-drag generator (MDG) rings

3.2.2.2 Wind Tunnel Test Setup

The drag device test was conducted in the Glenn L. Martin Wind Tunnel at the University of Maryland, College Park. The test section is 7 feet 9 inches in height by 11 feet wide. The tunnel is capable of speeds up to 230 miles/hr, and uses a six-component yoke to measure all six force and moment coefficients. A sketch of the tunnel defining the axis system is shown in Figure 3-25.

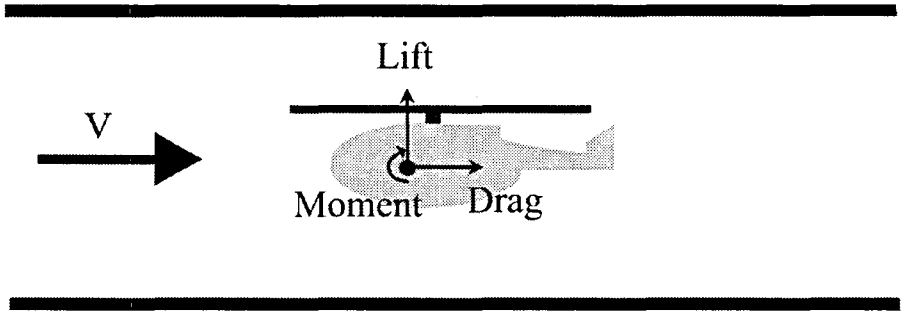

Figure 3-25. Sketch of wind tunnel axis system for lift, drag, and moment

The majority of the tests were run at a tunnel dynamic pressure, q, of 60psf, corresponding to a free stream speed V=235fps (155.7 miles/hr). This speed was chosen for two main reasons. Firstly, to ensure that buffeting effects were sufficiently small that they would cause no damage to the fuselage, and secondly to be operating at a velocity high enough such that C_D is no longer variable with Reynolds Number. There were two sets of runs that required lower speeds: a flow-visualization set and the split flap runs. For the flow-visualization runs, the presence of a human in the tunnel required that the velocity be decreased to 30mph. For the split flap runs the dynamic pressure of the tunnel was reduced to 23psf due to particularly strong buffeting that was shaking the tail.

Flow visualization was accomplished both by placing a smoke wand in the flow and by tufting the model. Tufts were used to provide flow-visualization at speeds that were too great for smoke. The model was tufted throughout the test program on the top and bottom surfaces, and on the side surface facing the wind tunnel cameras. The main objectives of flow-visualization were twofold: 1) determination of flow separation to find optimal area(s) in which to locate the drag devices, and 2) monitor the flow due to drag devices and their impact on both steady and unsteady loads and moments.

The scale model helicopter fuselage is 7.32 feet long by 1.40 feet tall by 2.09 feet wide. It is a 1 to 5.42 scale model of a modern full-sized helicopter. The model has a fairing (winglet) on either side of the fuselage, and has a vertical tail and horizontal stabilizer on the end of the tail boom (refer to Figure 3-19). The vertical tail was removed during the test so that the aerodynamic moments due only to the drag devices could be more appropriately investigated. The model had no rotor or hub, nor did it have a tail rotor.

3.2.2.3 Test Results and Conclusions

Detailed test results of the *x-force control* drag devices are contained in Appendix D. Measured force and moment coefficients are plotted for each drag device. The pattern and separation of the flow observed and visualized during testing are described. Their implications on lift, drag, side force, and pitching moment are also discussed. Finally, a derivation is provided by which calculations are made of the change in drag coefficients of all drag devices.

The experimental results demonstrate that the drag of a typical helicopter can be increased by substantial amounts while changing the helicopter force and moment balance in a controllable way. This strongly implies that BVI noise can be moderated by the addition of *x-force control* drag devices without having drastic control issues.

The micro-drag generator (MDG) devices were found to be the most promising for increasing helicopter drag. They increase the net drag of the fuselage while creating relatively small disturbance to the flow. They require less overall area than the other drag device concepts and their actuators would weigh less. Their location on the fuselage is critical, since they are only effective in regions on the fuselage where the flow remains attached. The test results of the micro-drag generator concept are encouraging enough to justify further investigations to determine it's overall feasibility on a full-scale helicopter.

The cone has the least effect on the flow around the fuselage since it is deployed back behind the tail. If it is brought closer to the tail boom of the fuselage, the cone can conceivably also be used as a safety device against the hazard of people walking into the tail rotor.

The split flap and flat plate devices act as drag brakes and are more difficult to use due to helicopter buffeting effects. They have massive impact on the flow no matter where they are

placed. Although these devices were over-designed, flaps and plates placed in the flow raise serious concerns about control issues, and these are only compounded when a tail rotor is added.

4. PHASE 2 IMPLEMENTATION PLAN FOR EVALUATION OF NOISE REDUCTION CONCEPTS

The selection of noise reduction concepts for evaluation in a Phase 2 effort is based on conclusions drawn from the Phase 1 noise reduction study. It has been found that the SILENT rotor design, incorporating the *modulated blade spacing* concept, offers significantly reduced noise levels and the potential of dramatically altering the perceptibility and subjective judgement of helicopter sound emissions. With these acoustic features, the SILENT rotor represents a definite advancement in the state-of-the-art. Hence, it is selected as the design concept for evaluation in Phase 2.

A Phase 2 Implementation Plan had been developed in which evaluations of a scaled model SILENT rotor are to be carried out in a whirl cage and in a wind tunnel. In the paragraphs below, the overall planning of these evaluations is discussed, the model rotor design and fabrication are described, the test facilities are identified, a test plan is proposed, and the estimated costs are summarized. Also, a projected schedule with major milestones is proposed for the Phase 2 effort.

4.1 Overall Planning

In planning for the evaluation of noise reduction concepts, NASA guidelines have been considered in that the cost of such evaluations should not exceed $1.3M. As a risk management tool, the total cost has been set at a not-to-exceed value of $1.1M. A preliminary cost analysis of designing, fabricating and testing three conceptual model rotors indicates that the target cost guidelines would be exceeded. Hence, alternatives have been sought.

It is desired to test three scale model rotors: a four-bladed rotor, a five-bladed even spaced rotor, and a five-bladed rotor with modulated spacing. Ideally, each of the rotors would have the same solidity. However, as indicated by the preliminary cost analysis, the cost of building all three rotors is prohibitive. An attractive alternative is to use existing blade assets from the Bell/NASA 8-foot diameter pressure instrumented rotor program. This rotor has been tested in the NASA LaRC 14 x 22-foot tunnel and there is an extensive database on the blades.

4.2 Model Fabrication

The hub will be redesigned to add a fifth blade to the rotor system to create the five-bladed rotor. The 5-bladed hub forces a larger radius than that of the baseline 4-bladed rotor, slightly changing several rotor characteristics as shown in Tables 4-1 and 4-2. A new hub is required for each rotor. The design would be based loosely on the existing hub design.

Table 4-1. Baseline Four-Bladed Model Rotor Characteristics

Radius	4.00-feet
Number of Blades	4
Chord	3.72-inches
Twist	-8 degrees
Thrust Weighted Solidity	0.098
Tip Speed @ 1695 rpm	710 fps

Table 4-2. Five Bladed Model Rotor Characteristics

Radius	4.08-feet
Number of Blades	5
Chord	3.72-inches
Twist	-8.16 degrees
Thrust Weighted Solidity	0.120
Tip Speed @ 1592 rpm	680 fps

The existing model rotor assets are shown in Figure 4-1. The rotor blades have integral cuffs and are fabricated from fiberglass and syntactic foam. Lead is used for section balance as necessary. The basic construction consists of a tapered fiberglass "D" spar with a foam core. The fiberglass plies in the spar have been tailored by material, ply build-up and ply orientation to match target spar properties. The after-body is fabricated from foam and the entire blade is skinned with two plies of fiberglass fabric as illustrated in Figure 4-2. A sufficient number of both pressure instrumented and non-pressure instrumented blades are available.

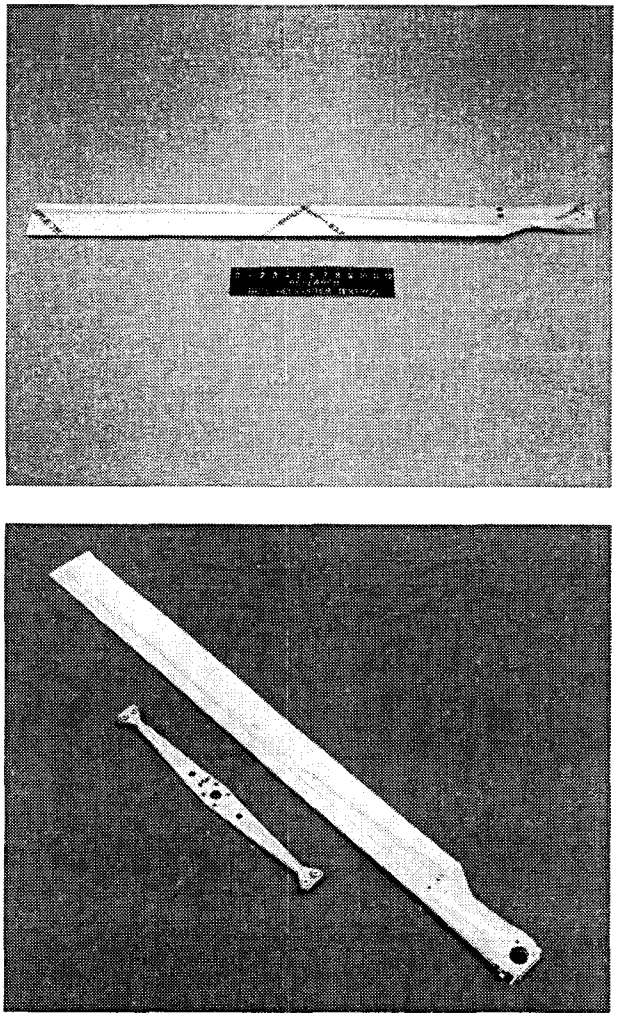

Figure 4-1. Existing model rotor assets

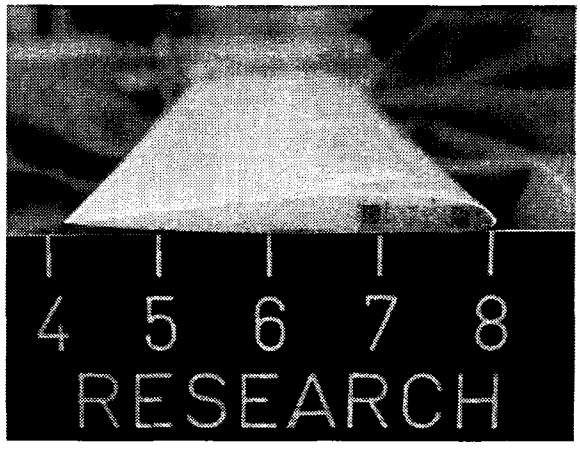

Figure 4-2. Model blade construction

The five-bladed rotor hubs would be designed such that the blades can be used without modification. One hub will be designed with even spacing. Another hub will be designed with the uneven spacing of the SILENT rotor design described in Section 3.2.1. A sketch of the hub design for the five-bladed rotor with *modulated blade spacing* is shown in Figure 4-3. All hub components are to be fabricated in the Bell Research Laboratory.

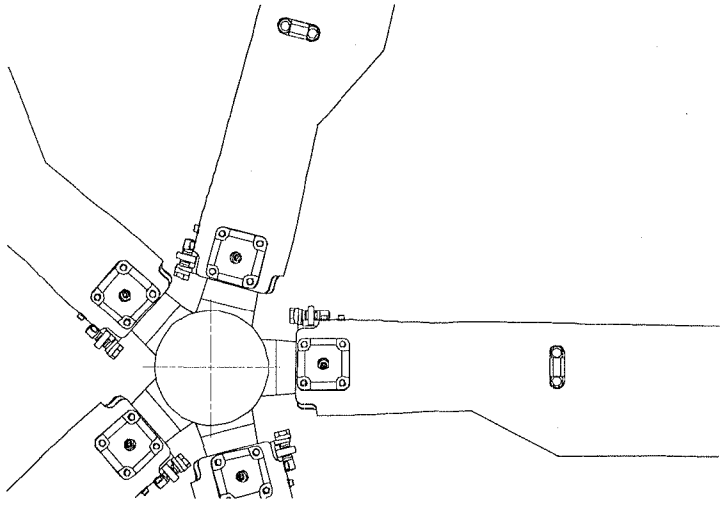

Figure 4-3. Sketch of hub design for rotor with modulated blade spacing

4.3 Test Facilities

The Bell Powered Force Model (PFM) is a general-purpose rotor test stand for testing Mach-scaled rotors. The PFM, shown in Figure 4-4, is capable of accepting rotors from 4 to 10 feet in diameter and operating at a maximum rpm of 3000. Two sets of spiral bevel input gears are available to maximize power available at the test rpm. The PFM is currently configured for the 2000-3000 rpm range. The proposed tests would require swapping the gear set for the lower rpm combination. The PFM utilizes two 75-hp drive motors rated at 75-hp each.

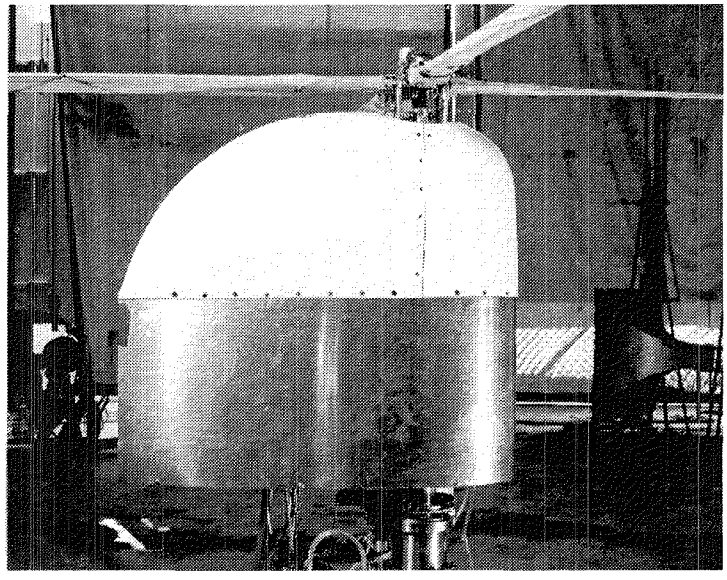

Figure 4-4. Powered force model (PFM) rotor test stand

The PFM is comprised of a drive motor, input quill assembly, pitch change mechanism, test stand dynamic isolator unit, five-component rotor balance and blade pitch controls. Pitch change takes place about the axis of the input quill assembly utilizing a remotely controlled pitch actuator. The isolator unit consists of four elastomeric dampers that can be adjusted, or locked out, depending upon the rotor frequency requirements. The PFM has a non-metric fairing designed minimize test stand interference with the rotor. The cross-sectional shape utilizes a NACA 0033 airfoil shape.

The five-component balance has the capability to resolve rotor forces into conventional forces and moment axes. Mast torque is obtained through a strain gage bridge located on the mast below the rotor hub attach point. A flex coupling which is designed to transmit minimal loads into the balance drives the rotor through the balance. The rotor cyclic and collective controls are mounted above the rotor balance. The PFM system is transportable with its motor power supply and re-configurable data acquisition system.

Before transporting, the PFM and complete model rotor system are to be thoroughly checked out and functional tests conducted in the Bell Research Hover Facility. This is a covered, vented facility with a full complement of power, instrumentation and model control systems that allows testing any time of the year. During these tests, the risk issues of blade tuning and loads will be addressed. Moving from four-bladed to five-bladed rotors may result in unattractive tuning and, consequently, higher blade loads. The five-bladed rotor with modulated blade spacing will be subjected to multiple, excitation loading frequencies.

After successful completion of the check out and functional testing, the model rotor system will be carefully disassembled. All lines, connectors, instrumentation harnesses, etc. will be marked and labeled to assure quick and reliable re-assembly for the wind tunnel test.

Primary testing of the scaled model rotors will be conducted at the NASA Langley Research Center 14 x 22-foot wind tunnel. This tunnel can be converted for acoustic testing, including installation of a traveling microphone array system. This allows multi-microphone measurements of each model rotor's noise behind, ahead and to each side.

4.4 Test Plan

After buildup in the test section of the NASA Langley Research Center 14 x 22-foot wind tunnel, all three scaled model rotors will be tested at comparable conditions. Emphasis will be placed on approach and level flight conditions.

The generalized test matrix planned for Phase 2 wind tunnel testing is shown in Table 4-3. Each rotor will be tested in seven test sets at conditions simulating level flight, takeoff and approach. In the level flight and approach testing, the tunnel velocity will be varied in increments from 50 to 90 knots. At each speed increment, the rotor angle of attack will be incrementally varied over

a range of −16 to +10/+12 degrees (+degrees aft). Thrust is to be held constant at 80% of the design hover thrust. Each rotor's design tip speed will be held constant at 100%. One test set is planned simulating approaches at low (30%) thrust. One other test set is planned simulating takeoffs at high (100%) thrust. It is estimated that 5-6 days will be required to perform the seven test sets for each of the three model rotor configurations.

Table 4-3. Generalized Test Matrix for Phase 2 Wind Tunnel Testing

Test Set	Nominal Velocity (kts)	Rotor Angle of Attack, (deg., +aft)	% Design Hover Thrust	Vtip
1	50	-16 thru + 12	80	100
2	60	-16 thru +12	80	100
3	70	-16 thru +12	80	100
4	80	-16 thru +10	80	100
5	90	-16 thru +10	80	100
6	60	-16 thru 0	100	100
7	60	-2 thru +12	30	100

4.5 Estimated Costs

In arriving at estimated costs, the basic tasks required to evaluate the noise reduction concepts have been identified and are listed below:

1. Conduct design trades to establish hub design approach
2. Conduct hub design and structural and dynamic analyses
3. Fabricate tooling and hub components
4. Issue test plan
5. Evaluate instrumentation on existing blade assets
6. Modify PFM and prepare for tunnel entry
7. Conduct whirl cage testing at BHTI
8. Pack and ship model system and DAS to LaRC
9. Build-up in tunnel
10. Conduct testing. (Assume tunnel is funded directly by Government)
11. Pack and ship to BHTI and prepare for storage
12. Issue wind tunnel data report
13. Provide administration, status reporting and attend briefings and coordination meetings

The man-hours and the material/vendor costs estimated to accomplish these tasks are summarized in Table 4-4. Both engineering (D81) and test laboratory (D86) man-hours are listed.

Table 4-4. Estimated Costs of Phase 2 Testing

Task	D81 Man-hours	D86 Man-hours	Material/Vendor
1	160	8	
2	900	24	
3	1000	80	$10,000.00
4	80	40	
5	16	80	
6	640	320	$4,800.00
7	480	160	
8	80	80	$2,500.00
9	200	160	$13,500.00
10	1120	336	$63,000.00
11	40	40	$2,500.00
12	640	160	
13	1120	____	$9,800.00
Totals	6476	1488	$106,100.00

4.6 Projected Schedule

The schedule projected for the Phase 2 implementation plan is shown in Figure 4-5. Approximately a 2-year effort is projected. The model design would start in the second quarter of 2002 and the final review would be held in the early part of the second quarter of 2004. The wind tunnel testing at NASA Langley Research Center is planned in the August-October 2003 timeframe.

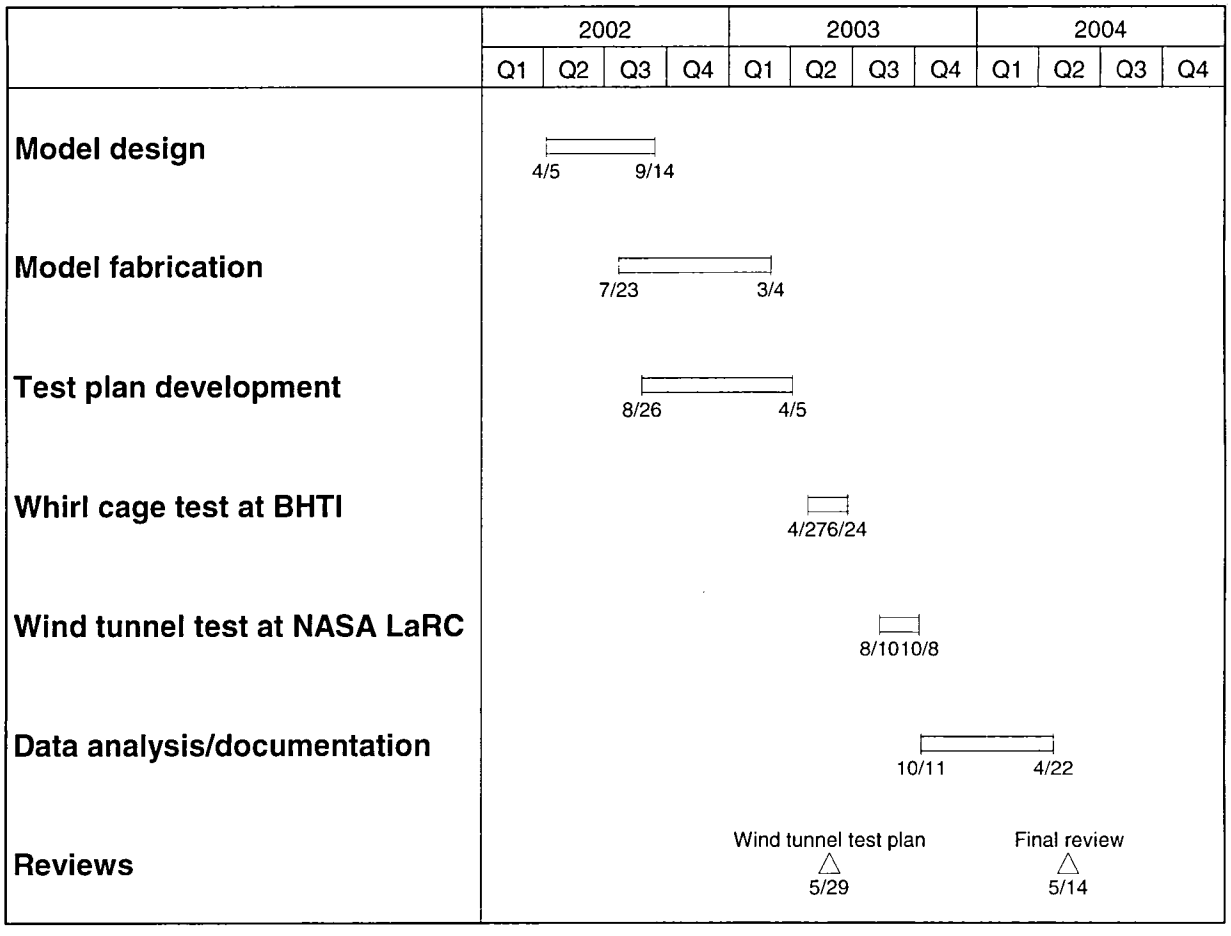

Figure 4-5. Schedule for Phase 2 Implementation Plan

5. SUMMARY AND CONCLUSIONS

The Phase 1 study of noise reduction concepts for helicopter main rotors has quantified the noise reduction potential and design implications of both conventional and novel acoustic design technologies. In the preliminary assessment of the concepts, first level analyses indicate significant noise reduction is possible with some of the concepts and when certain concepts are combined. Minimal impacts on performance and no increase in vibration are indicated, but design fundamentals must be followed. The first level analyses also clearly show that design modifications to the anti-torque system are typically necessary to fully realize the noise reduction potential of the main rotor noise reduction concepts. As a consequence of both main and anti-torque system modifications, each equally extensive in the cases analyzed, the baseline helicopter gross weight increases and the non-recurring costs and recurring production costs are higher.

The advantages/disadvantages and risk/payoff of each noise reduction concept have been assessed, leading to a down-selection of the most promising concepts. Two novel acoustic design technologies, *modulated blade spacing* and *x-force control* have been selected for further study because of their distinct advantages and their low-to-moderate risk and high payoff.

Evaluation of the *modulated blade spacing* concept includes detailed design of the rotor and an acoustic analysis. In the detailed design, the payload-range capability of a baseline rotor is matched to the extent possible. In evaluating various combinations of radius, chord and tip speed, it is shown that the main rotor diameter must be increased to improve hover performance enough to cover the growth in empty weight. Based on payload-range results, the configuration selected as the SILENT rotor has five blades, a radius of 19.5 feet, a thrust weighted chord of 12 inches, and a rotational tip speed of 665 feet per second. The SILENT rotor incorporates *modulated blade spacing* with angles between blades of 72, 68.5, 79, 65, and 76.5 degrees. If incorporated on the baseline helicopter, the SILENT rotor results in a 16 percent payload penalty for the full fuel case. The cruise airspeed would be reduced by 6.2 percent and the maximum airspeed by 17.2 percent.

In the acoustic analysis of the *modulated blade spacing* concept, the SILENT rotor's geometric parameters have been modeled analytically in the noise prediction program WOPWOP. These parameters include the blade radial properties (chord, thickness, twist), forward and lateral orientation of the rotor, blade flapping, collective and cyclic pitch, and lift and drag forces. To model the unique aspects of the SILENT rotor, the standard version of WOPWOP has been modified in three ways: to enable long observer time runs, to allow user input of the angles between the blades, and to utilize a unique loading data set for each blade.

On an A-weighted sound pressure level basic, the acoustic analysis clearly shows the SILENT rotor to be significantly quieter than the baseline rotor. The reduction in peak noise levels (three-microphone average) is predicted to be 4, 8 and 4 dBA during takeoff, flyover and

approach, respectively. The noise reductions up-range (15-20 seconds before overhead) are even greater: 16, 16 and 9 dBA during takeoff, flyover and approach, respectively.

When compared to an even-spaced five blade main rotor, the peak noise levels of the SILENT rotor average quieter by 2-3 dBA during flyover and approach, but average louder by 3 dBA during takeoff. Up-range the SILENT rotor is consistently predicted to be quieter, by 2 to 5 dBA, than the even-spaced rotor at all three flight conditions.

In addition to being quieter, the SILENT rotor's acoustic pressure time histories are strikingly different from those of even-spaced five-blade rotor and the four-blade baseline rotor. Such a difference indicates a fundamental change in how the SILENT rotor will be perceived and its sound judged, both from a community acceptance standpoint and from a military perspective. This feature of the SILENT rotor appears to offer a way, unique to the *modulated blade spacing* concept, to favorably alter a helicopter's sound signature. Computer files have been produced of the SILENT rotor's predicted acoustic pressure time histories. These files have been stored on a CD-ROM and are suitable for audio playback. In additional an audio simulation methodology has been developed that provides an automated means to generate audio wave files for any type of rotor configuration. All these files are available for sound quality assessments – a needed and intriguing follow-on study.

Evaluation of the *x-force control* concept involves wind tunnel experimental tests of four types of drag devices on a scale model helicopter fuselage. During testing, the helicopter's flight moment balance has been closely monitored via measurements of all forces and moments produced by each drag device. Also, flow visualization using a smoke wand and tufts is used to define the flow patterns and any flow separation caused by the drag device.

The *x-force control* experimental results demonstrate that the drag of a typical helicopter can be increased by substantial amounts while changing the helicopter force and moment balance in a controllable way. Micro-drag generator devices have been found to be the most promising way of increasing the drag of a helicopter. Such devices increase the net drag of the fuselage while creating relatively small disturbance to the flow. They require less overall area than the other devices and their actuators would weigh less. They are only effective in areas where the flow remains attached to the fuselage; hence, locating them correctly is critical.

Rationale for selection of design concepts for demonstration in a Phase 2 effort is based on conclusions drawn from the Phase 1 noise reduction study. It is concluded that the SILENT rotor design, incorporating the *modulated blade spacing* concept, offers significantly reduced noise levels and the potential of a break-through in how a helicopter's sound is perceived and judged. With all its acoustic features, the SILENT rotor represents a definite advancement in the state-of-the-art and is selected as the design concept for demonstration in Phase 2.

A Phase 2 Implementation Plan has been developed for whirl cage and wind tunnel evaluations of a scaled model SILENT rotor. In this plan, the overall planning is discussed, the model rotor

design and fabrication are described, the test facilities are identified, a test plan is proposed, and the anticipated costs are summarized. Finally, a projected schedule with major milestones is proposed for the Phase 2 effort.

It is also concluded that BVI noise can be moderated by the addition of *x-force control* devices without having drastic control issues. The test results of the micro drag generators are encouraging enough to justify further investigations to determine their overall feasibility. These investigations should be conducted on a full-scale rotorcraft; hence they are currently beyond the scope of Phase 2.

Finally, it is shown that the study's noise reduction targets have been met or exceeded in two of the three flight conditions. In level flight, the SILENT rotor is predicted to be quieter by 8 dBA compared to the 3 dBA target relative to the baseline design. During climb, the SILENT rotor is predicted to be quieter by 4 dBA compared to the 3 dBA target. During an approach, the SILENT rotor is predicted to be quieter (by 4 dBA) than the baseline design, but misses the target of 8 dBA. The noise reduction in approach may be under predicted since the effects on BVI noise of the SILENT rotor's tip shape could not be fully investigated analytically; hence, the need for the Phase 2 experimental testing. It is concluded that the current study has made a significant step in reaching the NASA Aeronautics and Space Technology Enterprise goals to reduce perceived noise levels of future rotorcraft.

REFERENCES

1. Edwards. B., Andrews, J., Rahnke, C., "Ducted Tail Rotor Designs for Rotorcraft and Their Low Noise Features," Paper 18 presented at the AGARD Flight Integration Panel Symposium on Advances in Rotorcraft Technology, Ottawa, Ontario, Canada, 27-30 May 1996.

2. Riley, R. G., "Effects of Uneven Blade Spacing on Ducted Tail Rotor Acoustics," presented at the AHS 52nd Annual Forum, Washington, D. C., 4-6 June 1996.

3. Andrews, J. R., Riley, R. G., Rahnke, C., "Design and Testing of a Ducted Tail Rotor Concept Demonstrator for a Model 222U Helicopter," Paper 4 presented at the 22nd European Rotorcraft Forum and 13th European Helicopter Association Symposium, Brighton, England, 17-19 September 1996.

4. Schmitz, F. H., "Reduction of Blade-Vortex Interaction (BVI) Noise through X-Force Control," Journal of the AHS, January 1998.

5. Gopalan, G., Schmitz, F. H., Sim, B. W., "Flight Path Management and Control Methodology to Reduce Helicopter Blade-Vortex Interaction (BVI) Noise," presented at the AHS Vertical Lift Aircraft Design Conference, San Francisco, California, January 2000.

6. Brentner, K. S., "Prediction of Helicopter Discrete Frequency Noise - A Computer Program Incorporating Realistic Blade Motions and Advanced Acoustic Formulation," NASA TM-87721, October 1986.

7. Brentner, K. S., Marcolini, M. A., Burley, C. L., "Sensitivity of Acoustic Prediction to Variation Of Input Parameters," Journal of the American Helicopter Society, Vol. 39, No. 3, pp. 43-52, July 1994.

8. Bauer, S. X., "An Aerodynamic Assessment of Micro-Drag Generators (MDGs)," presented at the 16th AIAA Applied Aerodynamic Conference, Albuquerque, New Mexico, June 1998.

APPENDIX A
ROTOR NOISE SIMULATOR METHODOLOGY

LIST OF FIGURES

PAGE

APPENDIX A
ROTOR NOISE SIMULATOR METHODOLOGY

Appendix A documents the methodology used in the development of a rotor noise simulator to produce rotor sounds that correspond to specified percent modulation blade spacing.

Baseline Waveform Development

In order to produce realistic rotor sounds, an audio recording of a helicopter flyover was used in the development of a baseline waveform. The baseline waveform was used as the basic building block for all generated waveforms.

The first step was to analyze the baseline waveform to determine which main and tail rotor frequencies were present. Using the acoustic analysis program SIA-SMAART, an FFT was made as shown in Figure A-1 from the first one half second of the recorded flyover. The measured main rotor frequencies are 31 Hz, 63 Hz, 95 Hz, 126 Hz, 159 Hz, etc. Tail rotor frequencies are 191 Hz, 285 Hz, 381 Hz, 476 Hz, and 565 Hz. The acoustic pressure waveform corresponding to this FFT is shown in Figure A-2.

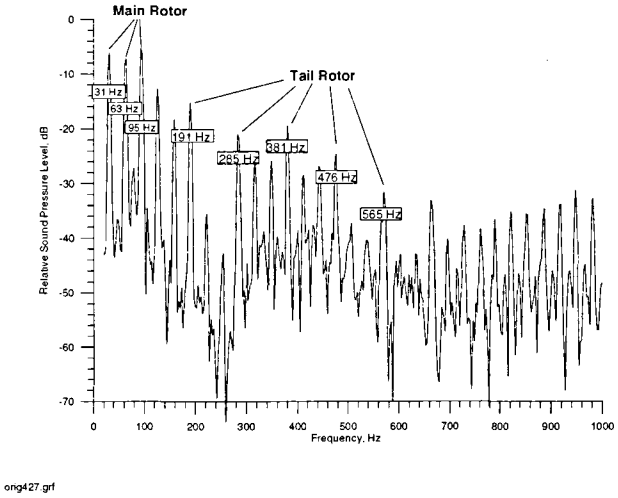

Figure A-1. FFT of helicopter flyover

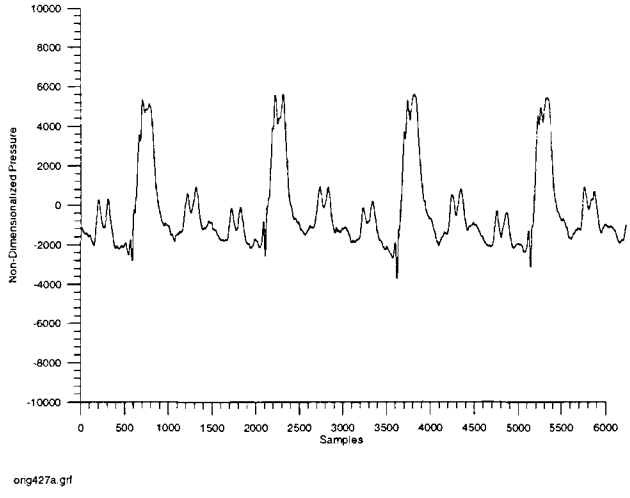

Figure A-2. Acoustic pressure waveform of helicopter flyover

The next step involved removing the tail rotor frequencies from the spectrum. This was accomplished using Cool Edit Pro and applying 5 parametric filters at 191Hz, 285Hz, 381Hz, 476Hz, and 565Hz with an attenuation of 20dB and a Q of 200 to the file "*wave1.wav*." This was then saved as "*wave2.wav*" and opened in SIA-SMAART to obtain the new FFT and the modified acoustic pressure waveform, as seen in Figures A-3 and A-4, respectively.

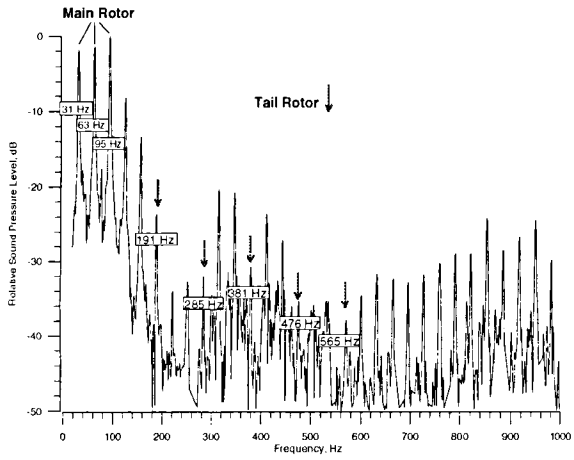

Figure A-3. FFT of helicopter flyover with tail rotor frequencies attenuated

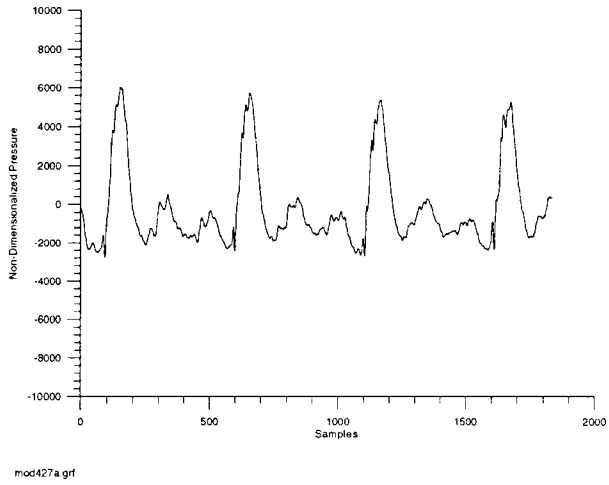

Figure A-4. Modified acoustic waveform with tail rotor frequencies attenuated

The "*wave2.wav*" file was then edited using Cool Edit Pro to obtain a single cycle of the acoustic pressure wave. The leading portion of this wave, originally consisting of fairly low amplitude pressure fluctuations, was replaced with 13 milliseconds of zero amplitude samples. This was done so that the spacing between pressure pulses could be reduced or increased in an automated manner to simulate the spacing of the desired design. Figure A-5 shows the final wave shape, denoted as the Super Wave, which is saved in the file "*Super.dat.*"

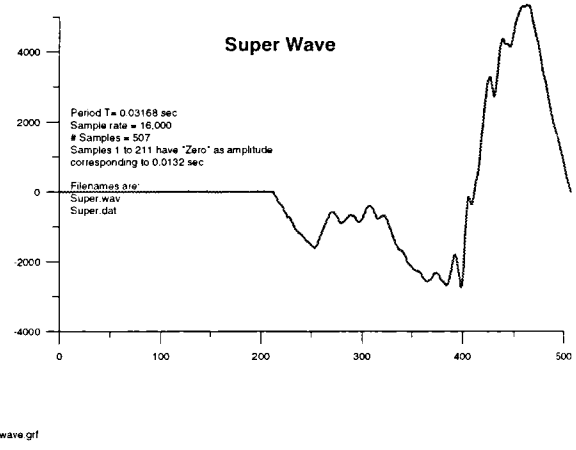

A-5. Super Wave – basic building block for waveform generation

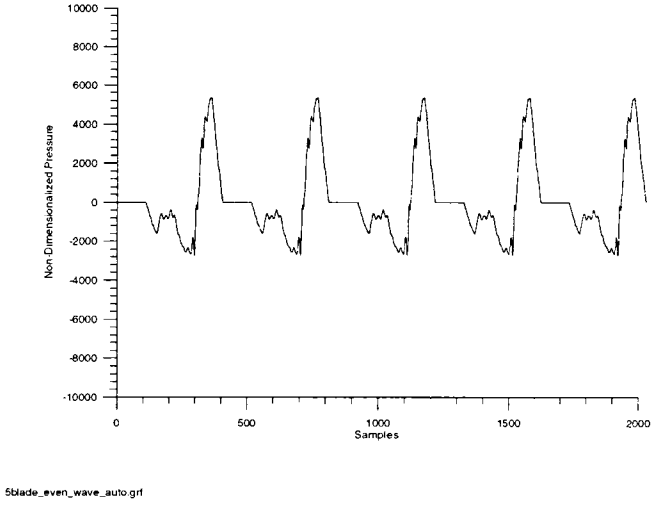

Figure A-6. 5 blade even spaced rotor acoustic waveform generated by automated program

Uneven Blade Spacing Simulation

In order to simulate the angular distance between unevenly spaced blades, the baseline waveform was replicated and the spacing between pulses was adjusted accordingly. This was accomplished in steps as described below.

First, the measured period of the baseline waveform was determined to be 0.03168 seconds. This corresponds to a fundamental blade passage frequency of 31 Hz for the helicopter's 4 blade main rotor. One complete rotor revolution would be (0.03168) * (4) = 0.12672 seconds. For a 5 blade main rotor with even spaced blades and at comparable rotational speeds, the period between pulses would be (0.12672) / (5) = 0.0253 seconds.

Second, to manually obtain an even spaced 5 blade rotor design, a 0.0064 second segment (0.03168 minus 0.0253 seconds) was cut from between two pulses and the remaining portion saved. This wave shape was then replicated to make the even spaced 5-blade rotor.

Third, uneven spaced wave shapes were then generated manually. Using an Excel chart, the delta time spacing for various uneven spaced blade configurations were calculated. Then the Cool Edit Pro cut and paste editor was used to modify the spacing between waveform pulses, thereby generating new waveforms for all uneven spaced blade configurations.

Finally, sets of wave files were created representing various main rotor designs. One set of wave files contains several identical pulses representing two even spaced configurations, a 4 blade and a 5 blade design; and five uneven spaced 5 blade designs with 5%, 7.7%, 10%, 12% and 15% modulation. Each of these wave files was then replicated 50 times, creating a second set which contains approximately five-second samples of each design for playback evaluation.

Automated Waveform Generation

Acoustic waveform generation was automated and programmed into the computer. The starting point for the generation of the audio simulation is the specified blade spacing in seconds, assuming a known rotational speed. For each blade spacing, the difference between the baseline wave *Super.dat* and the desired blade spacing in seconds is determined. Next the number of samples corresponding to this time is determined. This number of samples is then subtracted from the baseline wave's number of samples, in this case 211, having an amplitude of zero to obtain the final number of zero amplitude samples.

The blade spacing and wave information derived above were combined to form a *Blade Spacing and Waveform Generation* program. To verify that the program functions as planned, two cases were run. In each case, the results using the automated *Blade Spacing and Waveform Generation* program were compared with those made through the manual process of editing the waveform.

The first case was the 5 blade even spaced rotor. This corresponds to a percent modulation of 0%. The acoustic waveform generated by the automated program is given in Figure A-6. The corresponding waveform generated by manual construction is shown in Figure A-7.

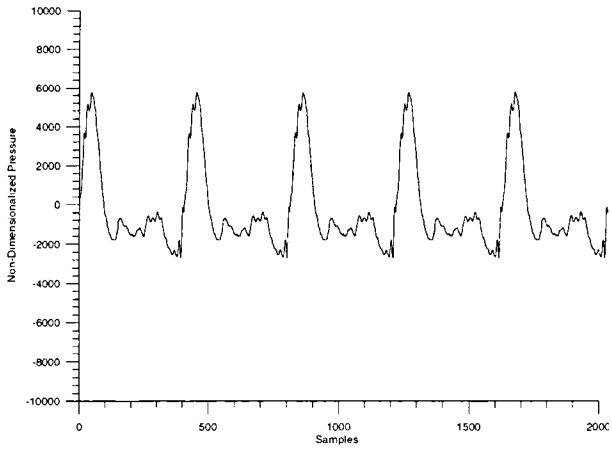

5blade_even_wave_manual.grf

Figure A-7. 5 blade even spaced rotor acoustic waveform generated by manual construction

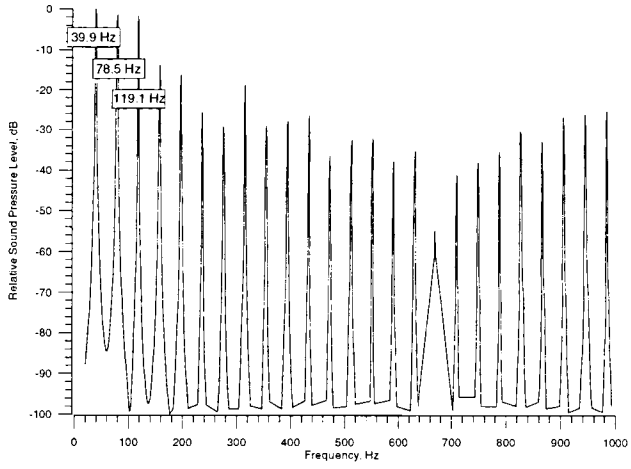

5blade_even_freq_auto.grf

Figure A-8. 5 blade even spaced rotor acoustic spectrum generated by automated program

By comparing Figures A-6 and A-7, it can be seen that the waveform generated by the automated program has the correct time spacing between pulses. Also, the pulses' rise time, peak shape, and decay history are identical for both methods of waveform generation. There are slight differences in the two waveforms between pulses, however, these are low amplitude and do not affect the results. Figures A-8 and A-9 show the corresponding spectra generated by the two methods of waveform generation. It can be seen that the two spectra are almost identical, with the exception of some additional low amplitude side-band peaks in the spectrum of Figure A-9 from the manual method.

In the second case, a final check of the program was made by evaluating an uneven spaced blade design. For this comparison a 10% modulation was chosen. The resulting acoustic waveforms and spectra using the two methods are shown in Figures A-10 through A-13. Again, the spacing between waveform pulses matches well for the two methods.

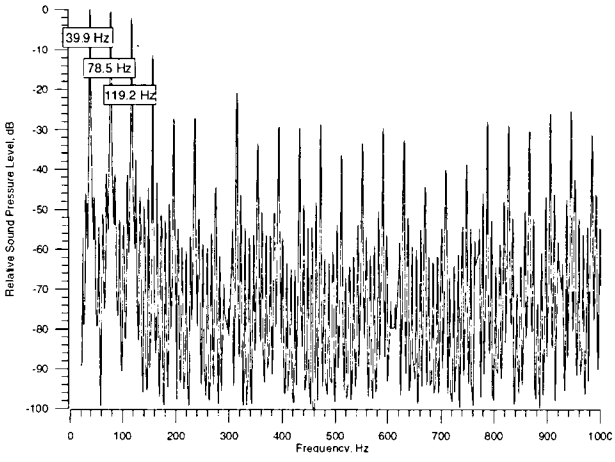

Figure A-9. 5 blade even spaced rotor acoustic spectrum generated by manual construction

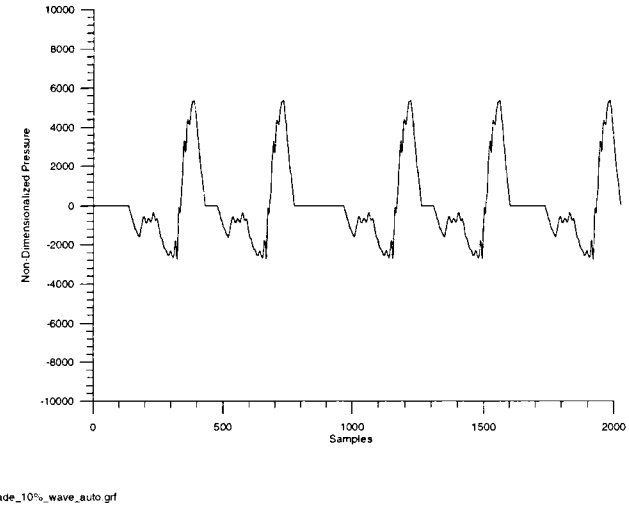

Figure A-10. 5 blade 10% modulation rotor acoustic waveform generated by automated program

The spectra shown in Figures A-12 and A-13 are nearly identical as well. Thus the automated *Blade Spacing and Waveform Generation* program is duplicating the desired blade spacing, pulse shapes, and spectral content. This gives confidence that a SILENT rotor design can be readily simulated and its acoustic waveform accurately analyzed.

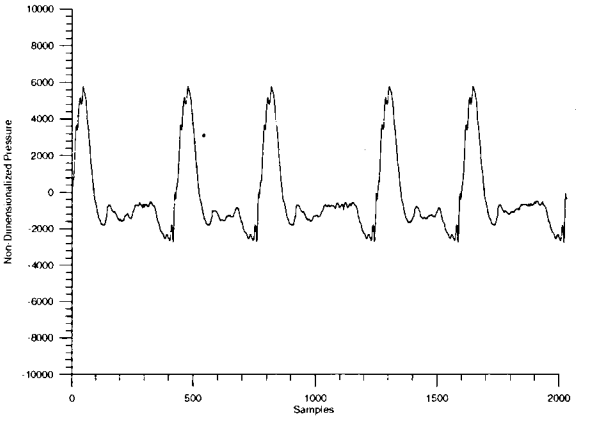

Figure A-11. 5 blade 10% modulation rotor acoustic waveform generated by manual construction

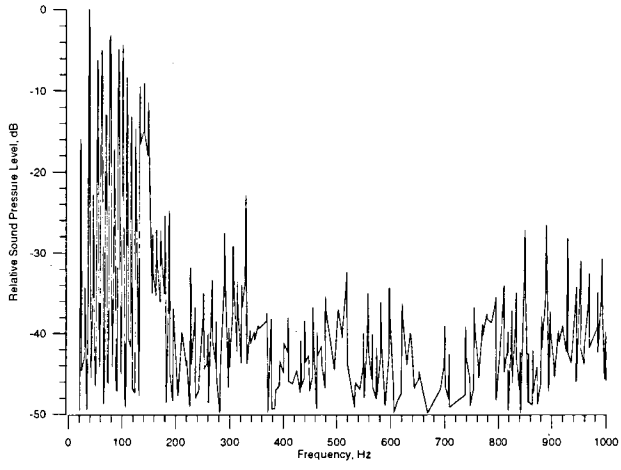

Figure A-12. 5 blade 10% modulation rotor acoustic spectrum generated by manual construction

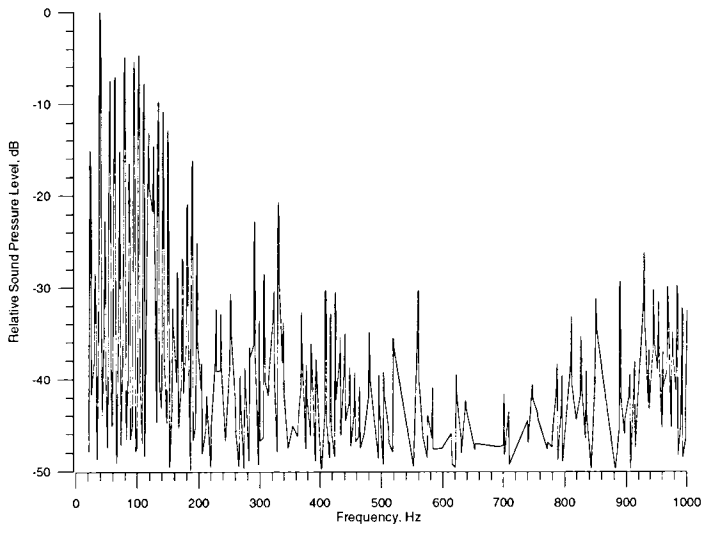

5blade_10%_freq_auto.grf

Figure A-13. 5 blade 10% modulation rotor acoustic spectrum generated by automated program

APPENDIX B
AERODYNAMIC DESIGN OF SILENT ROTOR CONFIGURATIONS

APPENDIX B - LIST OF FIGURES

PAGE

APPENDIX B - LIST OF TABLES

APPENDIX B
AERODYNAMIC DESIGN OF SILENT ROTOR CONFIGURATIONS

Assumptions

In the aerodynamic design of the SILENT rotor, the primary aim was to provide a practical design and match the payload-range capability of the baseline rotor to the extent possible. The following assumptions were used to evaluate the payload-range capability:

1) The evaluation should be done at a reasonably high density altitude, but not one that drives the design to extreme results. For this study, 6000 ft ISA conditions were assumed.

2) The mission profile was 5 minute HOGE at takeoff power, cruise at best range speed, and 20 minutes fuel reserve at best range speed.

3) HOGE power required was based on LSAF analysis for all rotors.

4) Cruise power required was based on COPTER analysis for all rotors.

5) Engine fuel flow was based on M427 HANDBOOK database tables.

6) The weight empty was based on the M427 Technical Info booklet.

7) Changes in weight empty for each configuration were based on PRESTO methodology. The weight empty was changed for component weight changes. The weight of the main rotor, mast, transmission, control system, and vibration suppression system were evaluated for each rotor configuration.

8) The M427 engines (PW207D), transmission power rating (800 eshp), and fuel quantity (203.5 gallons usable) were held constant for all configurations.

9) The cruise speeds of the SILENT rotor candidates were limited by empirical retreating blade stall boundaries. This assumption lowered the cruise speed, but did not have a large impact on the specific range.

10) The M427 non-dimensional twist and airfoil distributions were used for all rotor candidates.

Configurations Evaluated

Various combinations of chord, radius, and tip speed were evaluated. The basic design approach was to increase the diameter to improve rotor hover performance enough to cover the growth in empty weight. The most significant configurations evaluated are described below.

The payload-range was evaluated at 6000 ft ISA conditions. The M427 is transmission limited to 800 ESHP when using takeoff power. Table B-1 shows the HOGE performance (relative to the M427 baseline) for each configuration assuming the same transmission rating of 800 ESHP. The increase in weight empty is shown, along with the net payload penalty (again, both are relative to the M427 baseline).

Table B-1. Performances Comparison

Blades	ΩR (fps)	Radius (ft)	Thrust weighted chord (inches)	Solidity	Increased HOGE capability (lbs)	Increased weight empty (lbs)	Payload penalty (lbs)	Cruise speed (ktas)
4 (M427)	765	18.5	10.6	0.0610	-	-	-	129
5	650	18.5	20.0	0.1434	-257	1073	1330	~129
5	665	18.5	12.0	0.0860	46	289	243	117
5	665	19.0	12.0	0.0838	131	335	204	120
5	665	19.5	12.0	0.0816	220	382	162	120

For 6000 ft ISA conditions the M427 has a cruise speed of about 129 ktas and a V_H of ~145 ktas. The 20" chord design can match the V_H and probably would have about the same cruise speed. For the 12" chord designs, the cruise speed is also V_H.

The payload-range results for the baseline rotor and four SILENT rotor configurations are plotted in Figure B-1. Of the low tip speed rotors, the 19.5 ft radius has the best payload-range capability. Using the methodology described above, it appears that rotor radius greater than 19.5 ft will further reduce the payload penalty. But rotor radii larger than 18.5 ft will have clearance problems with the tail rotor, tail-boom, and endplates if incorporated on the M427 fuselage. The larger rotors will require an increased mast length and stretched tail-boom to provide clearance. The PRESTO weight methodology does not have the resolution required to capture these weight increases, so they are not incorporated in the aircraft weight empty. The SILENT rotor study was limited to 19.5 ft because the aircraft empty weight estimates would not be reliable for larger rotors.

SILENT Rotor Configuration

Based on the payload-range results, the baseline rotor and four SILENT rotor configuration selected as the SILENT rotor has five blades, 665 feet per second tip speed, thrust weighted chord of 12 inches, and a radius of 19.5 feet. The SILENT rotor uses the non-dimensional M427 airfoil and twist distribution. The chord distribution and quarter chord offset (positive aft) are listed Table B-2.

Table B-2. SILENT Rotor Blade Chord Distribution and Quarter Chord Offset

Radius, ft	Chord, ft	C/4 Offset, ft
2.02	1.059	0.0000
18.68	1.059	0.0000
18.76	0.979	-0.0060
18.85	0.821	-0.0177
18.96	0.628	-0.0146
19.07	0.475	0.0223
19.17	0.379	0.0876
19.26	0.330	0.1633
19.33	0.302	0.2304
19.46	0.174	0.3556
19.50	0.038	0.4123

A plot of the plan-form with the swept ogee tip shape is shown in Figure B-2. The rotor incorporates modulated blade spacing, with angles between the five blades of 72, 68.5, 79, 65, and 75.5 degrees.

The payload-range comparison of the SILENT rotor and the baseline rotor is shown in Figure B-1. If incorporated on the M427, the SILENT rotor would have a payload penalty of 162 lbs. With full fuel, this is about a 16% loss in payload compared to the baseline M427. Compared to the M427, the SILENT rotor's cruise speed would be reduced to 120 ktas from 129 ktas. Compared to the M427, the SILENT rotor's V_H speed would be reduced to 120 ktas from 145 ktas.

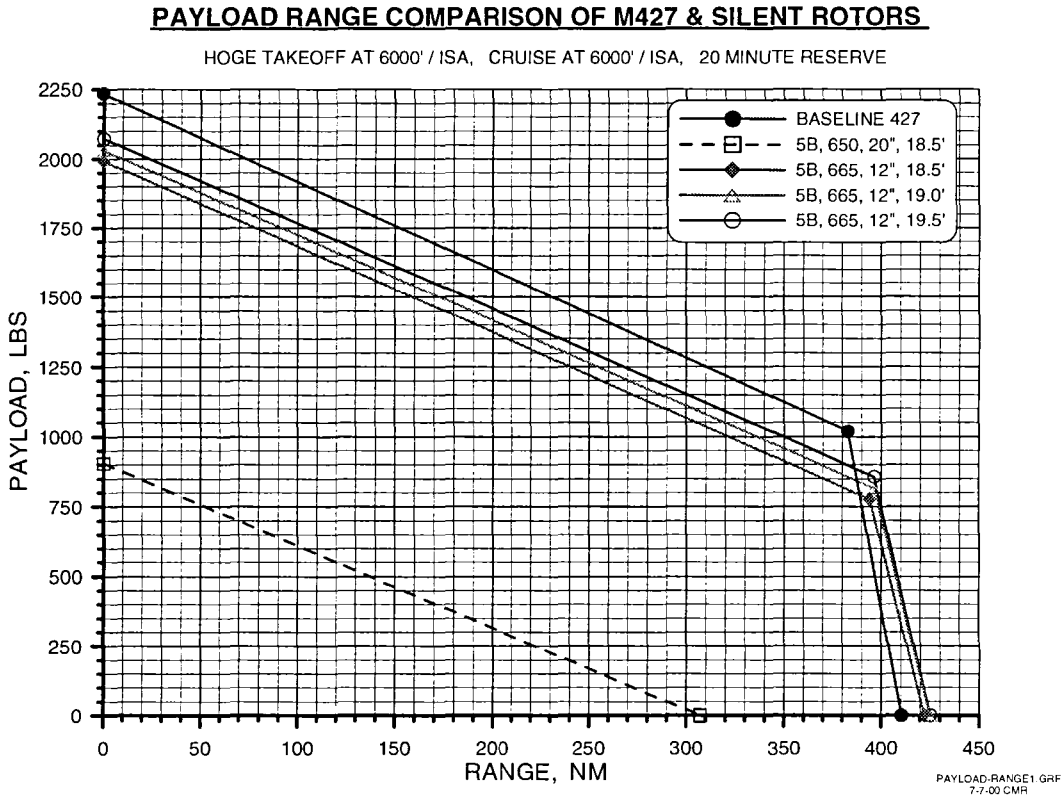

Figure B-1. Payload-range of baseline rotor and four SILENT rotor configuration

COMPARISON OF M427 AND SILENT ROTOR BLADES

	M427	SILENT
Number of Blades	4	5
Tip Speed, fps	765	665
Thrust weighted chord	10.6"	12.0"
Radius	18.5'	19.5'
Solidity	0.0610	0.0816

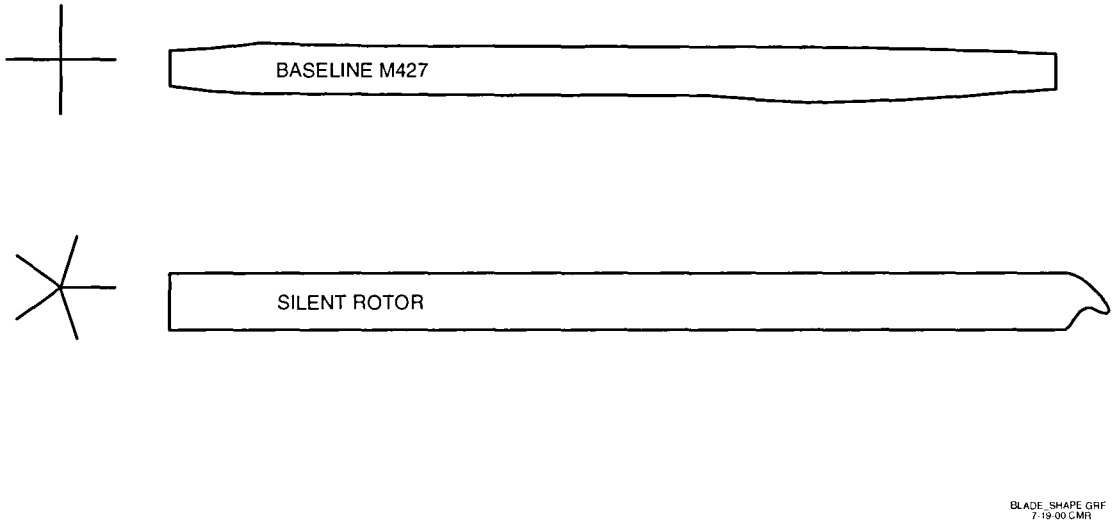

Figure B-2. Comparison of blade plan form of baseline and SILENT rotors

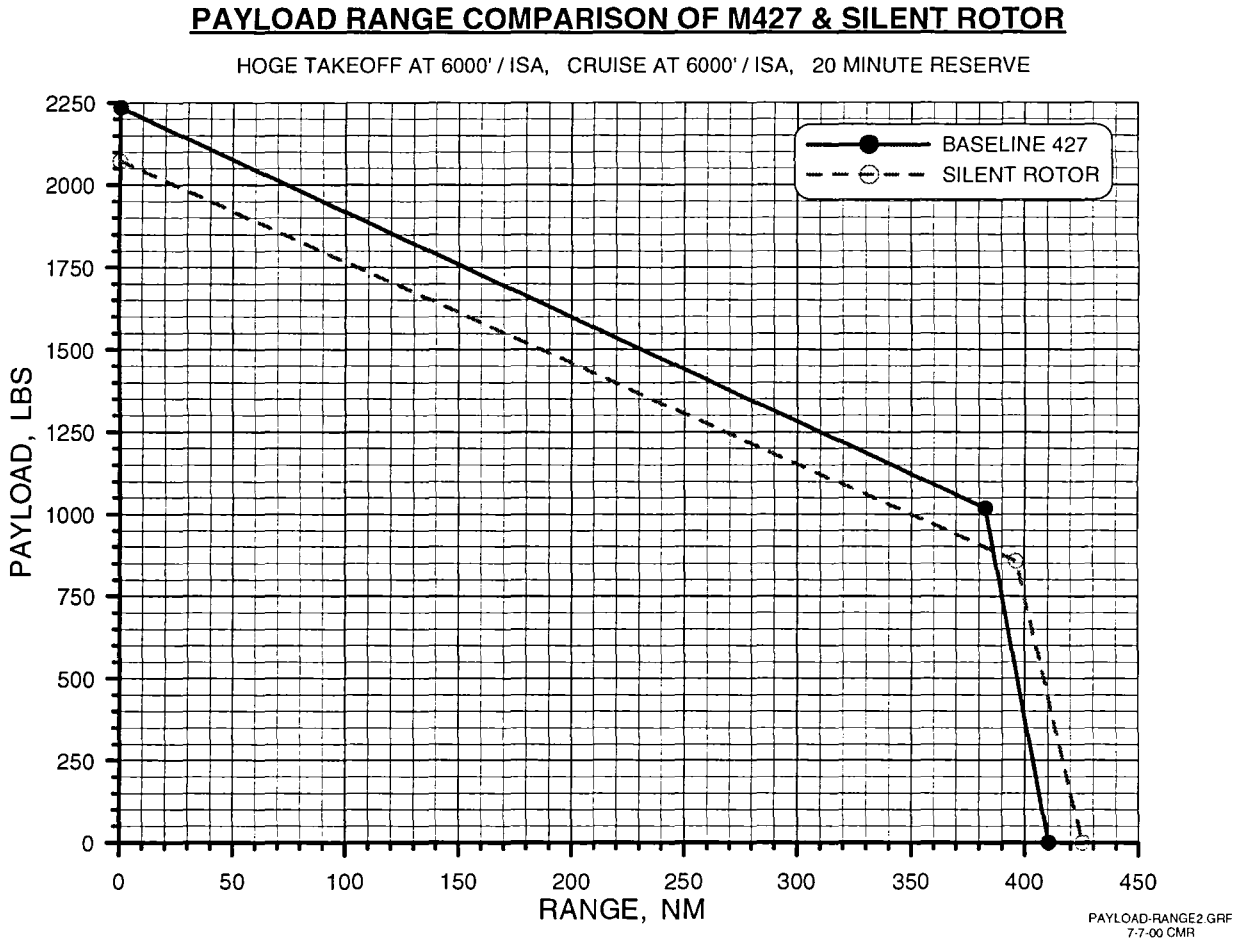

Figure B-3. Payload-range of baseline rotor and SILENT rotor

APPENDIX C
AUDIO PLAYBACK FILES AND CD-ROM

APPENDIX C
AUDIO PLAYBACK FILES AND CD-ROM

Audio Playback Files

The files are RIFF files written in WAVE format (more commonly known as "wav" files) which can be played on both UNIX and MS Windows platforms with a variety of players. The data format is written using 16 bits per sample at a sample rate of 48000 samples per second (one of the standard data rates for wave files). Since the acoustic prediction does not provide the acoustic pressure at this sample rate, interpolation (linear) is utilized. (The sample rate in the file is critical to ensure that the frequency content of the predicted signal is reproduced correctly.) The amplitude of the signal is adjusted to utilize the full range of the 16 bits, but the amplitude range is chosen such that all the cases have the same relative amplitude – i.e., cases can be compared on a volume basis.

Wave files in a directory labeled "MaxAmpWav" (in the Wave Files directory) have not been adjusted to have a common amplitude, but are useful for listening to the individual rotor signals. The rotor signals in these wave files are primarily low frequency, therefore, it is important to have a reasonable subwoofer on the playback computer.

CD-ROM

The CD-ROM is written by a PC with an MS Windows operating system (Windows 98, 2nd edition). The main level directory contains a copy of this final report in MS Word 2000 format, along with directories (folders) entitled "Acoustic Pressure Time History Files," "SPL Time History Files," "Tecplot Layout Files," and "Wave Files." In each directory (except "Tecplot Layout Files)" are subdirectories labeled "427 Rotor," "SILENT_Even" and "SILENT_Modulated," respectively, which contain the results for the three different rotor configurations. The "Wave Files" directory also contains a subdirectory "MaxAmpWav" which also contains the three subdirectories with wave files that are not based on a common amplitude setting.

In a rotor director (427 Rotor) for example, there are 9 files – one for each microphone and flight condition combination. The files begin with the label "M427," "SE" or "MO" which indicates the 427 rotor, SILENT evenly spaced rotor, or SILENT modulated rotor, respectively. (This notation is a duplication of the directory structure.) The file names then contain two digits, "fo", "to", or "ap" which indicates the flight condition – i.e., flyover, take off, or approach. Next are two digits indicating the microphone – M1, M2, or M3. In the directory for the SPL time histories, the filenames also have the letter LA to differentiate between a SPL time history and an acoustic pressure time history. The files either have a ".tec" extension to indicate a TECPLOT readable file or ".wav" extension to indicate a WAVE format audio file.

In the directory "Tecplot Layout Files," packaged data layout files of each of the figures used in this report. Packaged data layout files contain the data and the style – so the figure can be recreated just by opening the layout with TECPLOT. These files are provided to assist BHTI in modifying the format of the plots (if required). TECPLOT version 8.0 was used to generate the plots and these packaged data layout files.

The acoustic pressure time history data files are written as an ASCII file in TECPLOT format, with 9 variables: t, T_f, T_n, T, L_f, L_n, L, O, I, which are the observer time, far-field thickness noise, near-field thickness noise, thickness noise, far-field loading noise, near-field loading noise, loading noise, total (combined) noise, and the index, respectively. These files can be examined using tecplot and could easily be post processed – i.e., to use the flight test data system to compute SPL time history for example.

The SPL time history data files are also written as an

ASCII file in TECPLOT format, with 5 variables: time, OASPL, OASPL (no window), OASPL A, OASPL A (no window) which correspond with observer time, Overall SPL time history, Overall SPL time history without the Hanning window, A-weighted SPL time history, and A-weighted SPL time history without the Hanning window.

APPENDIX D
TEST RESULTS OF X-FORCE CONTROL DRAG DEVICES ON A SCALE MODEL HELICOPTER FUSELAGE

APPENDIX D - LIST OF FIGURES

PAGE

APPENDIX D - LIST OF TABLES

APPENDIX D
TEST RESULTS OF X-FORCE CONTROL DRAG DEVICES ON A SCALE MODEL HELICOPTER FUSELAGE

Clean Configuration: The baseline C_D of the model was 0.2782 at α=0°, β=0°. At α=0°, β=-6°, the baseline C_D was 0.3079. The drag coefficient is based on a frontal reference area of S_w = 1 ft^2. (Note: On the graphs all the baseline data are shown in dark solid lines.)

Cone: Figure D-1 shows the force and moment coefficients for the cone at a yaw angle of 0°. The drag increase due to the cone was measured as 234% over baseline. The coefficient of drag for the cone went to 0.9291 for the α=0°, β=0° case.

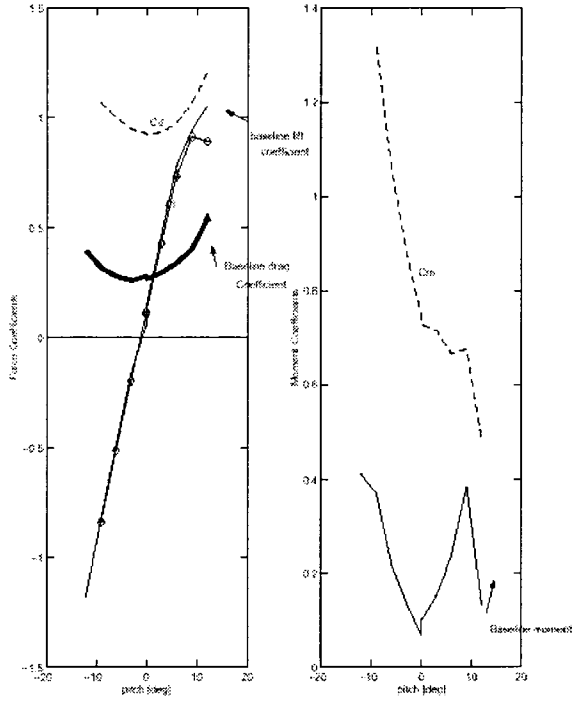

Figure D-1. Force and moment coefficient for cone

The drag from the cone is due mainly to the sudden pressure drop at the edges of the cone causing massive pressure drag. At 0° pitch, 0° yaw, the lift and side forces remained nearly the same as in the baseline case. This is in accordance with the theory of flow over a symmetric body, which puts forth that there should be no lift or side forces at 0° angle of attack. As the fuselage is yawed, the lift trend starts to differ from the baseline as the flow over it becomes unsymmetrical. A similar effect is felt as the fuselage is pitched. The cone had a significant impact on the helicopter's stability. A 200% increase in pitching moment was recorded when the cone was deployed. The increase in pitching moment is mainly due to the resultant drag force not passing directly through C_g. There is some moment arm between the resultant drag

addition and the C_g, which causes a net pitch down moment. The change in pitch moment starts to increase as the cone is yawed. The increase with yaw appears to be due to the fact that the cone is generating lift and drag forces that act with a greater moment arm about C_g.

Split Flap Simulator: The split flap simulators had to be run at q=23 psf due to the enormous unsteadiness they generated over the control surfaces and tail. The results in Figure D-2 show an overall drag increase of 548% over the baseline case at $\alpha=0°$, $\beta=0°$. The strips effectively act as a large split drag brake and are enormously effective at generating drag. Flow separates on the rearward surface of each strip and causes a somewhat large pressure drag. The split flap idea was used because it was thought that it would have something less of an impact on the flow that a single large flat plate. The separation between the strips was also thought to allow flow to pass through the split flap, again slightly reducing the impact of the device on the flow. Despite that, the flow turbulence and resulting buffeting were still overwhelming.

The split flap also destroyed lift over the fairings to a great degree as shown in Figure D-2. The placement of the devices was intended to mimic the actual position in which a real split flap would be deployed. For that reason, they were placed over the top of the fairing. As expected, putting a series of flat plates overtop of a lifting surface decreases significantly the lifting capability -in this case a decrease of 50% lift between the baseline case and the split flap run. Pitching moment for the split flap was also relatively large. The additional drag force located so far from the C_g generated significant nose up moment.

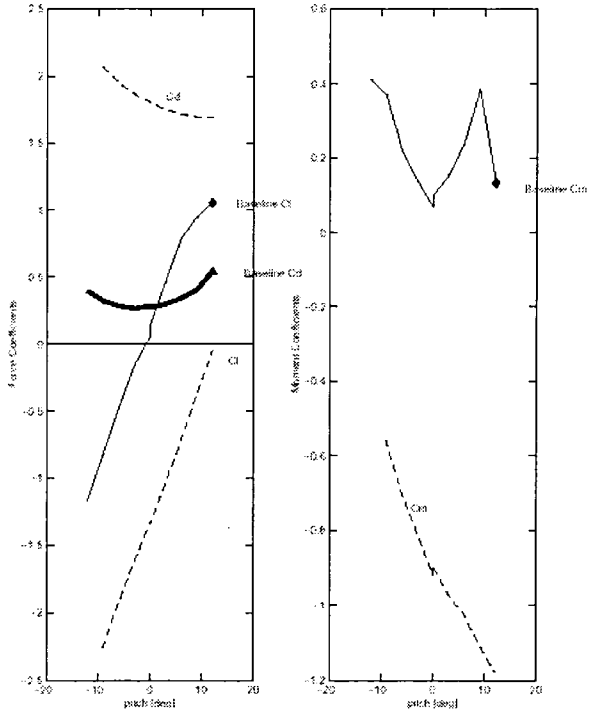

Figure D-2. Force and moment coefficient for split flap simulator

Single Flat Plate: The single flat plate under the fuselage, placed normal to the external flow, was effectively modeled as a simple drag brake. The idea is that a device such as this could be extended when the helicopter is on landing approach and could be deployed between the landing gear. The drag increase in this case was exactly the same as with the split flap simulator, 548%. The results shown in Figure D-3 are not surprising since both devices generate drag in the same manner and have the same projected area. Force and moment coefficient for split flap simulator devices was expected to have the same C_D. The lift was essentially destroyed when the single flat plate was placed in the flow. The flow separates immediately upon hitting the plate and caused the helicopter fuselage to lose nearly half of the baseline lift. The side forces slightly decrease, a phenomenon that is probably due to the plate being mounted slightly off-center on the bottom of the fuselage. The pitching moment was significantly altered by the placement of the plate on the belly of the model. Due to its position on the bottom-most surface, the drag produced by the single flat plate caused a large pitch down moment.

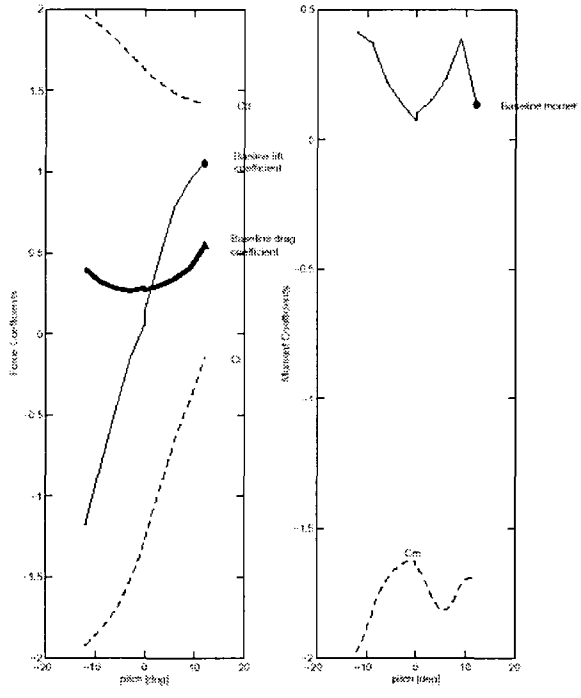

Figure D-3. Force and moment coefficient for single flat plate

Micro-Drag Generator (MGD) Devices: The (MDG) devices were envisioned to create a uniformly distributed drag force along the fuselage by forcing the flow to separate on the aft-facing surface of a series of deployable devices (small plates perpendicular to the flow). Since the flow needs to remain attached over the series of devices, they should be placed in areas where there is little or no adverse pressure gradient. Conceptually, the separated flow will cause

a two-dimensional vortex to be trapped behind the MDG. This causes a region of low pressure to be formed as shown in Figure D-4.

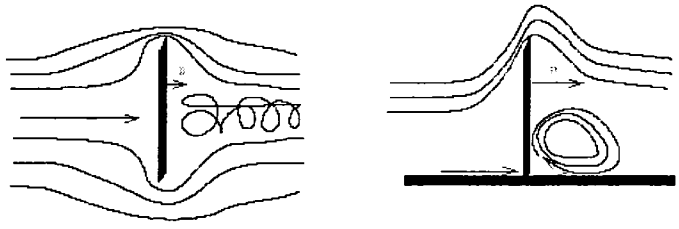

Figure D-4. Sketch of flat plate and MDG flow patterns

The vortex generates a low-pressure region on the downstream side of the plate, which effectively increases the pressure drag. Although small in magnitude, the drag force is quite large when normalized to the flat plate area. This is in contrast to the flat plate where drag is increased by separated flow. When deployed over the body, the total amount of drag generated by the MDG can become substantial.

A specific spacing between each set of devices must be maintained so that the separated flow coming off the front of a MDG will reattach before hitting the next MDG downstream. The drag generated by this system is equivalent to that which would be expected from a single flat plate device with larger projected area. Reference 8 describes how the height and width of the MDG cause variation in the amount of drag produced, as well as the rules for spacing plates to optimize drag generation. There are other benefits of having a number of small devices instead of one large device, mainly the associated reduction in the weight of actuators, increase in safety, and uniform distribution of load. The increase in safety comes about because several MDG devices could fail without having a large effect on drag generation capability. Hence, they are more robust and safer than flat plate concepts.

Due to the complexity of making a system of MDG devices work efficiently, several trial runs with different possible configurations were conducted. The first configuration was a simple combination of small plates arranged in series along the bottom of the fuselage. The plates were 6 inches long and 0.5 inch high with spacing between devices of 3.5 inches. The drag increase for this case was negligible over the baseline case, shown in Figure D-5. It appears as though there may have been significant 3-D effects in the form of a cross flow that tends to leak around the edges of the devices. The first runs also suffered because the flow was not reattaching on the aft side of the MDG arrays in the 3.5 inches between the devices, causing the MDG devices downstream to be bathed in the wake of those farther upstream. Without clean flow and an attached boundary layer, the MDG devices were ineffective at generating drag.

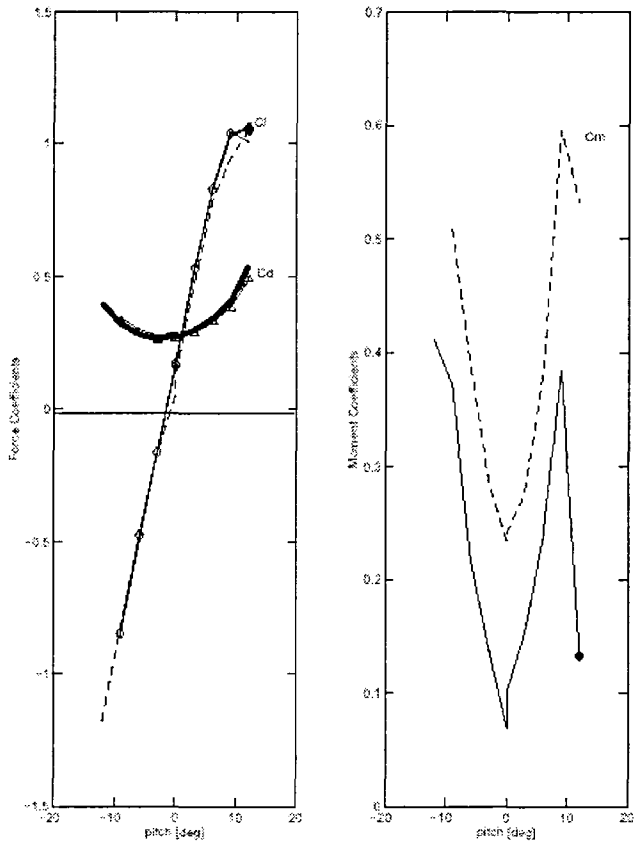

Figure D-5. Force and moment coefficients of non-ringed MDG devices

The configuration was changed after the fourth row of MDG devices proved ineffective. Instead of placing simple MGD strips, the fourth row was changed to a solid ring encircling the fuselage. This alleviated the problem of 3-D effects by reducing the ability of the flow to go around the edges of the plates.the results for one MDG ring are shown in Figure D-6 where there is a drag increase of 159% over the clean configuration. Another ring was then placed 3.5 inches downstream of the rearmost MDG. The measured drag increase was only 1% over the previous configuration as shown in Figure D-7. The flow did not appear to be reattaching, so the ring was shifted back another 3.5 inches for a total spacing of 7 inches between devices. This ring causes the drag to increase to 175% over the baseline case (a 15% increase over the previous run). The conclusion obtained from this case is that spacing is critical in making MDG devices effective, especially in 3-D flow. The test results seem to show that the spacing effects change considerably between 2-D and 3-D conditions.

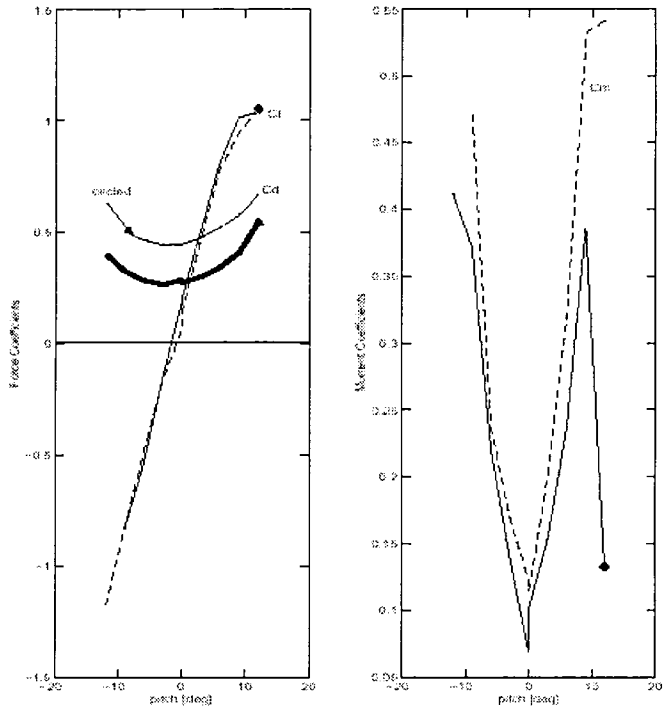

Figure D-6. Force and moment coefficients for one MDG ring

That is to say that the separation bubble behind a MDG in 3-D flow is larger than that expected in 2-D flow. More MDG devices were placed on the fuselage in areas where the flow is expected to be attached. The greatest drag occurred when a ring was placed around the fuselage and around the fairings. The results plotted in Figure D-8 show an increase in drag of nearly four times the clean configuration, in this case 376% increase, with less impact on the pitching moment than any of the other drag devices.

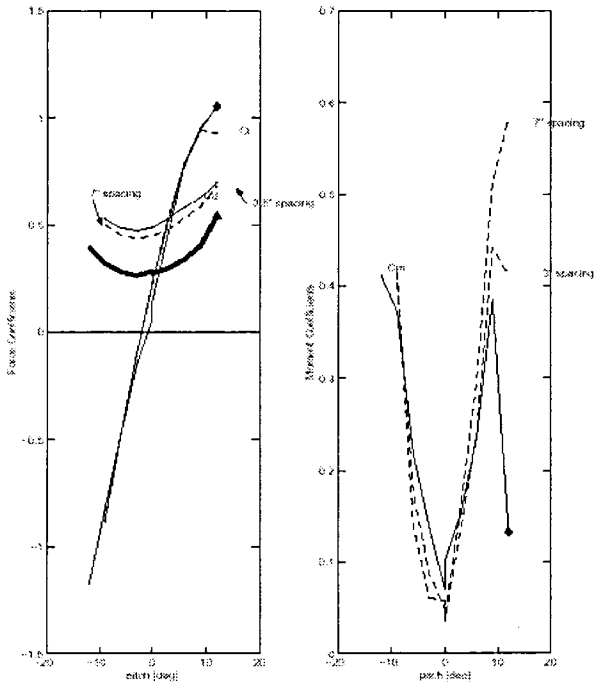

Figure D-7. Force and moment coefficients for increased MDG device spacing

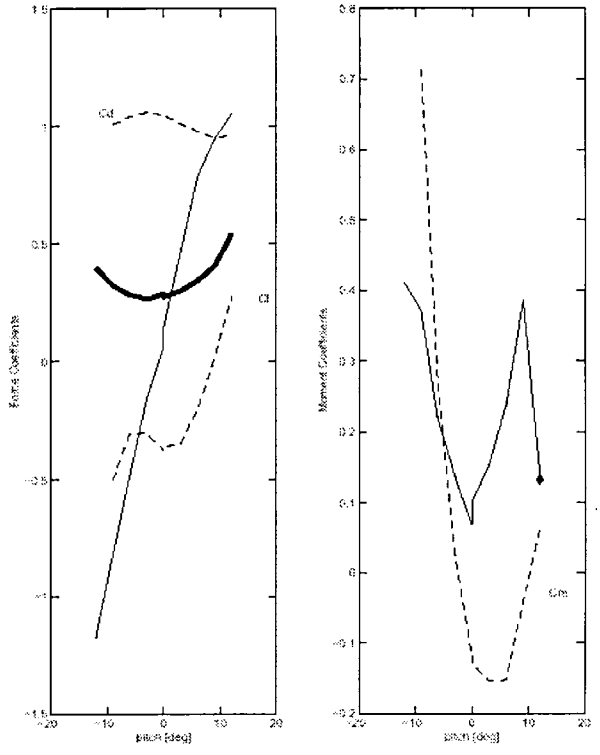

Figure D-8. Force and moment coefficients of final MDG device configuration

Derivation and Calculation of Change in Drag Coefficient

Further analysis was conducted to investigate whether a system of MDG devices work as drag generators or if the devices just increase the drag by adding more projected frontal area. The derivation shown below provides a method to calculate the effective change in drag coefficient of the devices referenced to their area. The drag measured by the tunnel force balance is referenced to the model area, S_{BM}.

The total drag of the baseline model and drag of the device is

$$D = 1/2\rho V^2 S_{BM} C_D \tag{D-1}$$

$$D_{Total} - D_{BM} + \Delta D \tag{D-2}$$

So

$$C_{D_{Total}} = \frac{D_{BM} + \Delta D}{1/2\rho V^2 S_{BM}} \tag{D-3}$$

And

$$\Delta C_{D_{W\_T}} = \frac{D_{Total} - D_{BM}}{1/2\rho V^2 S_{BM}} \tag{D-4}$$

Where $\Delta D_{D_{W\_T}}$ is the change in drag coefficient referenced to the fuselage reference area, and $\Delta C_{D_{Device}}$ is the change in drag coefficient due to the actual device. The change in drag coefficient referenced to the area of the drag device is

$$\Delta C_{D_{Device}} = \frac{\Delta D}{1/2\rho V^2 A_{Device}} = \frac{\Delta C_{D_{W\_T}} 1/2\rho V^2 S_{BM}}{1/2\rho V^2 A_{Device}} \tag{D-5}$$

Which becomes

$$\Delta C_{D_{Device}} = \frac{\Delta C_{D_{W\_T}}}{\frac{A_{Device}}{S_{BM}}} = \Delta C_{D_{W\_T}} \frac{S_{BM}}{A_{Device}} \tag{D-6}$$

Table D-1. Effective Change of Drag Coefficient for all Drag Devices

Drag Device	Area ft^2	$C_{D.Total}$	ΔC_D	$\Delta C_{D.device}$
MDG ring 1	0.18	0.445	0.167	0.93
MDG ring 2	0.12	0.489	0.044	0.36
2MDG on fairings	0.04	0.732	0.243	5.8
MDG ring 3	0.16	1.05	0.558	3.4
Split or long plate	0.50	1.80	1.53	3.06
Cone	0.92	0.929	0.651	0.71

This change in drag coefficient, normalized by the reference area, is important specifically to MDG devices. Using equation (6), the effective change of drag coefficient for all drag devices was calculated and is compared in Table D-1. As can be seen, when placed in the proper regions of the flow, MDG devices can be more effective at generating drag than flat plates. It is also important to note that the MDG devices have significantly less impact on the flow than the

flat plates. The success of the MDG devices is very dependent upon their location on the body. The rings placed early in the flow are much less effective than those placed over the fairings, and are not as efficient at drag generation as were the flat plates. The reason the first MDG rings are less effective is that they were all placed strictly normal to free-stream flow. To produce the most drag, the devices should all be mounted normal to expected local flows. In the current tests, there may have been significant local velocity gradients nonparallel to the free-stream. This may have caused delays in reattachment of the flow after it crests over a device and a corresponding loss in drag production. Overall, however, it should be noted that the best MDG device configuration had a significantly higher value $\Delta C_{D,device}$ than the flat plate. The probable reason for the higher value of $\Delta C_{D,device}$ is that the MDG devices are creating an induced vortex causing high rotational velocities behind the plate. The higher velocity associated with this vortex causes a pressure drop that increases the pressure difference between the front and back of a MDG device and causes an increase in pressure drag. This proves that it is feasible for an array of MDG devices to surpass flat plates in overall drag production using the same flat plate area.

REPORT DOCUMENTATION PAGE

Form Approved
OMB No. 0704-0188

1. AGENCY USE ONLY *(Leave blank)*	2. REPORT DATE	3. REPORT TYPE AND DATES COVERED
	May 2002	Contractor Report

4. TITLE AND SUBTITLE
Revolutionary Concepts for Helicopter Noise Reduction — S.I.L.E.N.T. Program

5. FUNDING NUMBERS
NAS1-99109

727-03-15-10

6. AUTHOR(S)
Bryan Edwards, and Charles Cox

7. PERFORMING ORGANIZATION NAME(S) AND ADDRESS(ES)
Bell Helicopter Textron Inc.
P.O. Box 482
Fort worth, TX 76101

8. PERFORMING ORGANIZATION REPORT NUMBER
699-099-529

9. SPONSORING/MONITORING AGENCY NAME(S) AND ADDRESS(ES)
National Aeronautics and Space Administration
Langley Research Center
Hampton, VA 23681-2199

10. SPONSORING/MONITORING AGENCY REPORT NUMBER
NASA/CR-2002-211650

11. SUPPLEMENTARY NOTES
Langley Technical Monitor: Earl R. Booth, Jr.

12a. DISTRIBUTION/AVAILABILITY STATEMENT
Unclassified–Unlimited
Subject Category 71 Distribution: Standard
Availability: NASA CASI (301) 621-0390

12b. DISTRIBUTION CODE

13. ABSTRACT *(Maximum 200 words)*
As part of a NASA initiative to reduce helicopter main rotor noise, a Phase 1 study has been performed of candidate noise reduction concepts. Both conventional and novel design technologies have been analyzed that reduce the community impact of helicopter operations. In this study the noise reduction potential and design implications are assessed for conventional means of noise reduction, e.g., tip speed reduction, tip shapes and airfoil tailoring, and for two innovative design concepts: modulated blade spacing and x-force control. Main rotor designs that incorporate modulated blade spacing are shown to have reduced peak noise levels in most flight operations. X-force control alters the helicopter's force balance whereby the miss distance between main rotor blades and shed vortices can be controlled. This control provides a high potential to mitigate BVI noise radiation. Each concept is evaluated using best practice design and analysis methods, achieving the study's aim to significantly reduce noise with minimal performance degradation and no vibration increase. It is concluded that a SILENT main rotor design, incorporating the modulated blade spacing concept, offers significantly reduced noise levels and the potential of a breakthrough in how a helicopter's sound is perceived and judged. The SILENT rotor represents a definite advancement in the state-of-the-art and is selected as the design concept for demonstration in Phase 2. A Phase 2 Implementation Plan is developed for whirl cage and wind tunnel evaluations of a scaled model SILENT rotor.

14. SUBJECT TERMS	15. NUMBER OF PAGES
Helicopter, acoustics, noise, rotorcraft, main rotor, BVI, modulated blade spacing, X-force control	86
	16. PRICE CODE

17. SECURITY CLASSIFICATION OF REPORT	18. SECURITY CLASSIFICATION OF THIS PAGE	19. SECURITY CLASSIFICATION OF ABSTRACT	20. LIMITATION OF ABSTRACT
Unclassified	Unclassified	Unclassified	UL

End of Document